Contents

List of Figures

Chapter 1

Introduction

1.1 Presentation

The principle of the Particle Tracking Velocimetry is one of the oldest way to evaluate the velocity of a fluid. It consists in determining the movement of a particle and knowing its position at different time, the velocity can be estimated. This technique was for a long time only applied with very few particles, as usually processed manually. But, with the development of computers, there has been a constant effort during the last two decades to build softwares able to track automatically particles. Nowadays, the number of particles that can be handled is growing and it is possible to treat images usually used for correlation technique. This paper intends as presenting the different steps required to implement a tracking software, together with typical applications and comparisons with Particle Image Velocimetry results. At the end, a particular application will be presented where the tracking of individual particles is the key point and where no correlation technique can give the proper results. The extension of PTV to PTV-Sizing will be presented and two-phase flow application will be presented.

1.2 Two-phase flows requirements

A two-phase flow is characterized by the simultaneous presence of different particles. A very important parameter is the knowledge of the size of the particle, as different behavior are expected depending on the size. There exists single point measurement to determine simultaneously the size and the velocity of the droplets. This kind of technique relies on the Doppler effect for the velocity and the deviation of light when passing through a medium of different index of refraction (Bachalo & Houser (1984)). The problem is that to understand some flow phenomena, an instantaneous field of view is more suitable. Therefore, there is a need to develop techniques able to measure those quantities.

1.3 The different steps required

To use PTV, one has to develop several image processing package in order to get the velocity. The first step is the detection of particles within the images. This is the key point as a bad detection may result in the wrong estimation of the proper displacements. If the constraint are too severe, only few particles may be detected, resulting in a poor spatial resolution. On the other hand, if one implements a too tolerant algorithm, it may result in tracking object that are not particles. The next chapter will discuss the different possibilities. After detection, one has to find the displacement between the two images. The chapter 4 will expose the different existing solutions. After, in chapter 5, a series of synthetic images are used to discuss the validity of the tracking and the different parameters that may influence the final results. In chapter 6, typical applications of tracking will be presented to illustrate the advantage of the tracking. Special attentions will be dedicated to the steady streaming displacement found in lungs bifurcation (section 6.2), where PTV is the suitable technique to give an answer to this problem. As this techniques intends to be applied to two-phase flow conditions, results obtained with water sprays will be presented in chapter 7. The PTVS can be applied to measure simultaneously the two phases. Two examples in chapter 8 will emphasize this aspect of the technique.

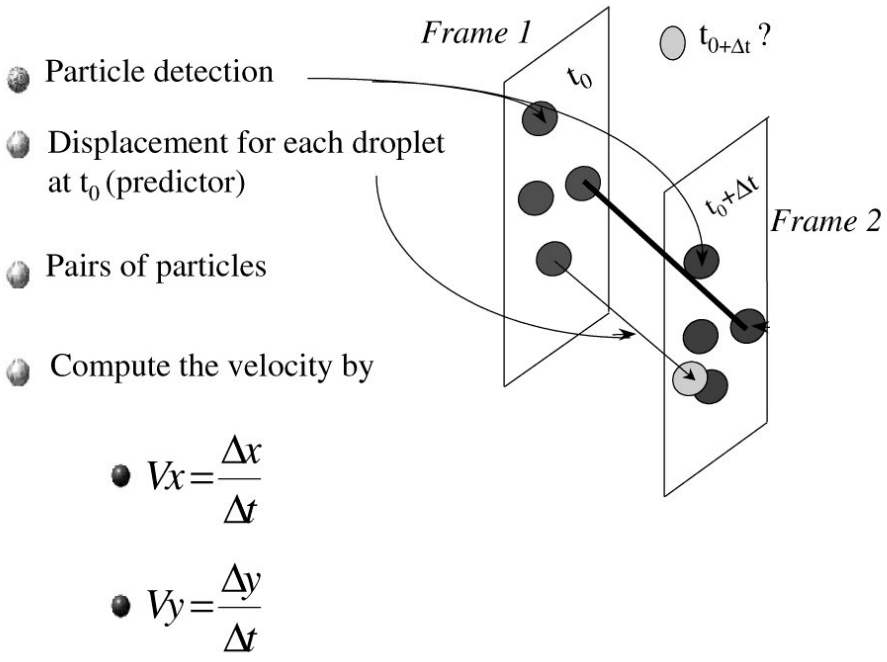

Figure 1.1: The two main steps for PTV treatment

Chapter 2

Detection

After the acquisition of the digital images, the first treatment to perform is the identification and localization of all the particles. There exists different ways to proceed and some of them will be exposed in the following sections.

2.1 Pattern recognition

Among the different possibilities, the pattern recognition technique is the most robust but also the most time consuming. The principle is to use a pattern, representing the light distribution within a particle. Afterwards, the correlation between this predefined pattern and all the images enlightens the centroids of the particles, as exhibiting a maximum of correlation. Usually, a pattern having a Gaussian distribution is used, as presented by Etoh *et al.* (1998). To clearly identify the centroids of particle, the normalized correlation coefficients (ranging from -1.0 to 1.0) are taken and only values above 0.7 give the center of the particle. This has to be imposed, to avoid spurious noise in the final results. The advantage of this technique is that noise is generally not taken into account when determining the position of the particles. But, its main drawback is that a single pattern can not be used, as two particles will seldom exhibit the same intensity on a digital image. Therefore, to take into account the different diffraction patterns, one should use different patterns, as presented by Kim *et al.* (1999). An application of a predefined pattern (see Figure 2.1(a)) with a synthetic image (see Figure 2.1(b)) is presented in figure 2.1(c) resulting in the identified particles presented in Figure 2.1(d).

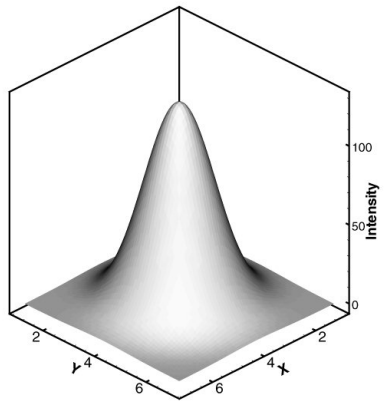

(a) Gaussian pattern used for detection

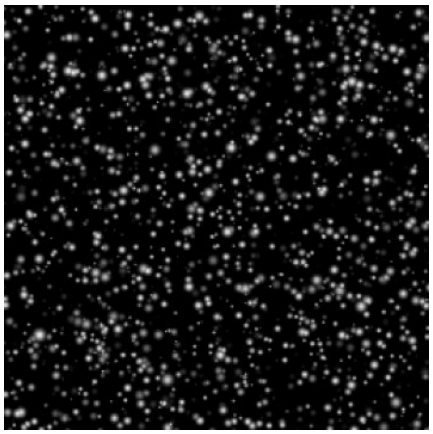

(b) Initial image to process

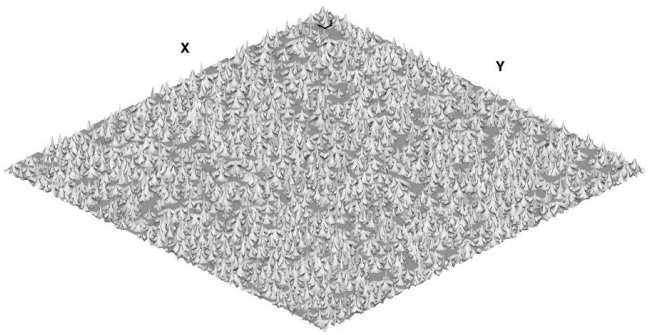

(c) Correlation map

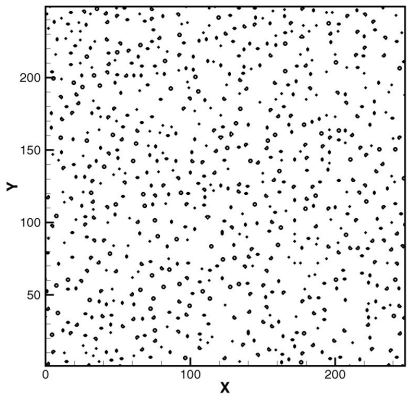

(d) Positions of particles

Figure 2.1: Use of a pattern to identify particles within an image

2.2 Contour detection

The basis for contour detection is that a particle should have a different intensity than the surrounding medium. Therefore, it should be possible to distinguish the boundaries of the particles. Usually, this kind of technique is done using mathematical operators that enhance the contours. Among the most used, one can cite the Sobel filter. The principle is to correlate the operator with the intensity image where the particles have to be found. The Sobel filter is defined in two ways (see equations 2.1 and 2.2), depending in which direction the gradient has to be enhanced. For detection purpose, the two definitions should be combined. This is a local filter as it takes only surrounding information to perform the detection. Hence, it could be sensible to local perturbations and should be used carefully.

$$Grad_y = \begin{bmatrix} -1 & -2 & -1 \\ 0 & 0 & 0 \\ 1 & 2 & 1 \end{bmatrix} \qquad (2.1) \qquad\qquad Grad_x = \begin{bmatrix} 1 & 0 & -1 \\ 2 & 0 & -2 \\ 1 & 0 & -1 \end{bmatrix} \qquad (2.2)$$

To illustrate how the detection is made, a simple case is presented when looking at vertical boundaries (applying $Sobel_y$). The matrix of the processed values begin with the point 2,2 from the original matrix.

20	20	19	23	25	18
19	20	22	21	19	22
20	23	43	66	50	19
22	19	54	90	58	21
21	21	47	61	39	23
18	22	21	19	22	20

Figure 2.2: Initial array of intensity

29	94	135	94
33	**132**	**209**	**146**
1	1	-17	-23
-31	**-134**	**-211**	**-144**

Figure 2.3: Processed array and peaks of contrast

For detection purpose, only absolute values are taken into account. As the Sobel operator only enhances the gradients, a threshold has to be fixed in order to determine the real boundaries of particles. Looking for maxima above this threshold give the boundaries in the vertical direction. A full example obtained with the Sobel filter is depicted on figure 2.4(a) and 2.4(b). Of course, it is possible to build new filters according to the type of results sought. The principle however remains the same : multiplying the matrix of the image by the matrix of the filter. One can fix higher orders of matrices for the definition of the filter. The main problem of such an approach is that the overlapping particles are not directly found, but they require a special treatment. For instance if there is a sudden change in the curvature of the boundary, this comes probably from overlapping droplets.

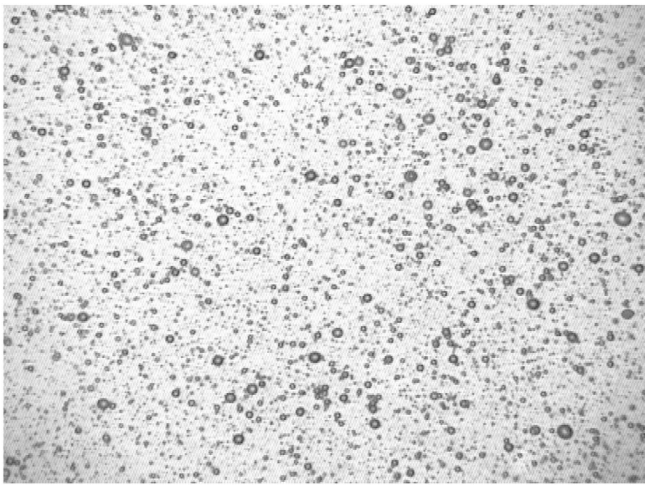

(a) Typical images with back-lighting technique

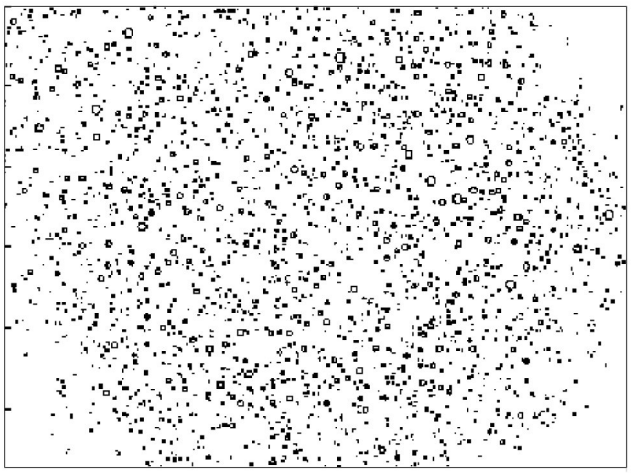

(b) Processed image with position of each bubble

2.3 Identification of centroids

Another possibility is to detect peaks of intensity within the image. Each peak is a possible center of a particle. In order to take into account non uniformity of the light and to avoid noise, there should be a dynamical determination of the level above which the peak is the center of a particle. Some neural networks (Ohmi & Li (2000)) may be used to determine the local threshold to use to discriminate between noise and particles. In the present case, the detection is done in two steps. The first one is to remove the mean value of the global image. Afterwards, the local threshold is estimated by computing the local mean value of the intensity and its RMS. The advantage of this procedure is that it enables to recognize overlapping particles very easily. This requires the presence of peaks of intensity for each particles. An example of an application of this technique is given in Figure 2.4. The initial image, showed in the left has particles that are overlapping. As seen on the processed image, it seems that the overlapped particles are well identified. When using a contour detection algorithm, this identification would require the determination of sudden changes of curvature to detect such group of particles. Its use is possible but requires more CPU time.

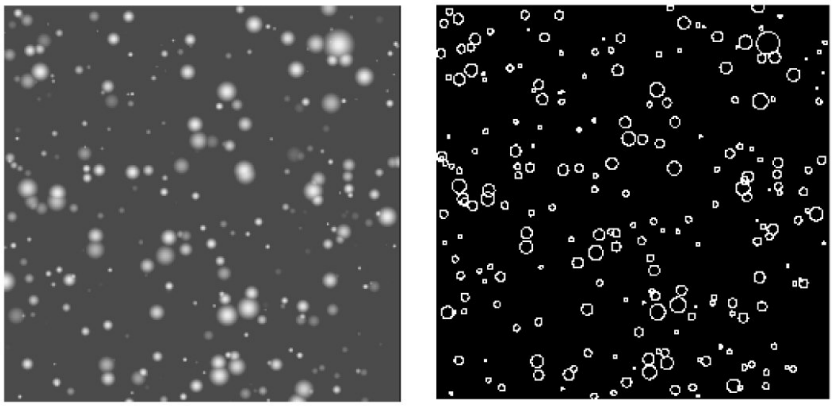

Figure 2.4: Detection by peak recognition

Chapter 3

Sizing

The need to have a technique giving real size of the droplets seem to be useful. The next chapter deals with the development of such algorithms.

3.1 Back-lighting digital sizing

For particles large enough, the size seen on an image can be assumed to represent the real size. For that purpose, the contour of the object has to be determined and gives the size. The original image (see Figure 2.4(a)), as well as the processed one (see Figure 2.4(b)).

An example of such a procedure is illustrated in Figure 3.1(a), where the sizes of bubbles presented in Figure 3.1(b) are determined.

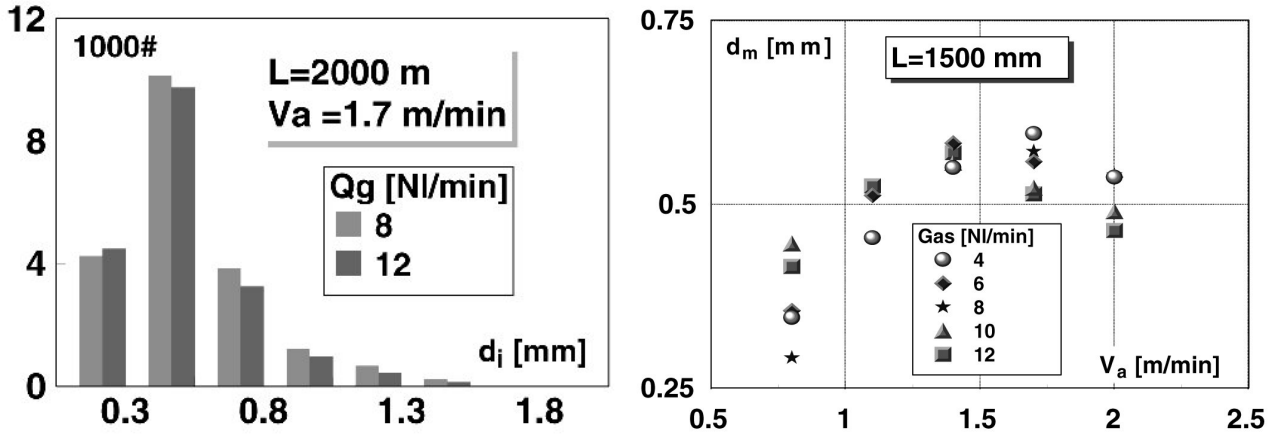

(a) Reference flow field

(b) Results of the tracking algorithm

Figure 3.1: Application of tracking on synthetic images

The major limitation of this technique is the low void fraction that can be processed.

3.2 Global intensity

Another possibility for measuring the size is to compute the global intensity scattered by the particle and to relate this to the size. But, two main problems arise when applying this to real images. The first one is the non-uniformity of the incident light through the image. Therefore, particles having the same diameter will not scatter the same amount of light. This could be solved by using a dynamic calibration for the incident light. The second problem arises when dealing with poly-distributed particles. To have a good dynamic range, it is

hard to avoid intensity saturation for the bigger particles. If the total intensity is considered, one can expect bad measurement in the higher range.

3.3 Gaussian profile

Instead of taking the global intensity scattered, it is possible to take the edges of the particle, as well as its center to compute the best Gaussian function through the different points. This case is also able to deal with plateau of intensity, the only problem in this case is the lower accuracy achieved in determining the center of the particle. The value of the threshold beyond which the particle is cut is influencing a little the determination of the size, as long as the particle is represented by more than 3 pixels. Below this limit, the measurement is too random and should not be performed. Therefore, when applying such a technique to real cases, one should look carefully to the size of the window used to see the range of diameters.

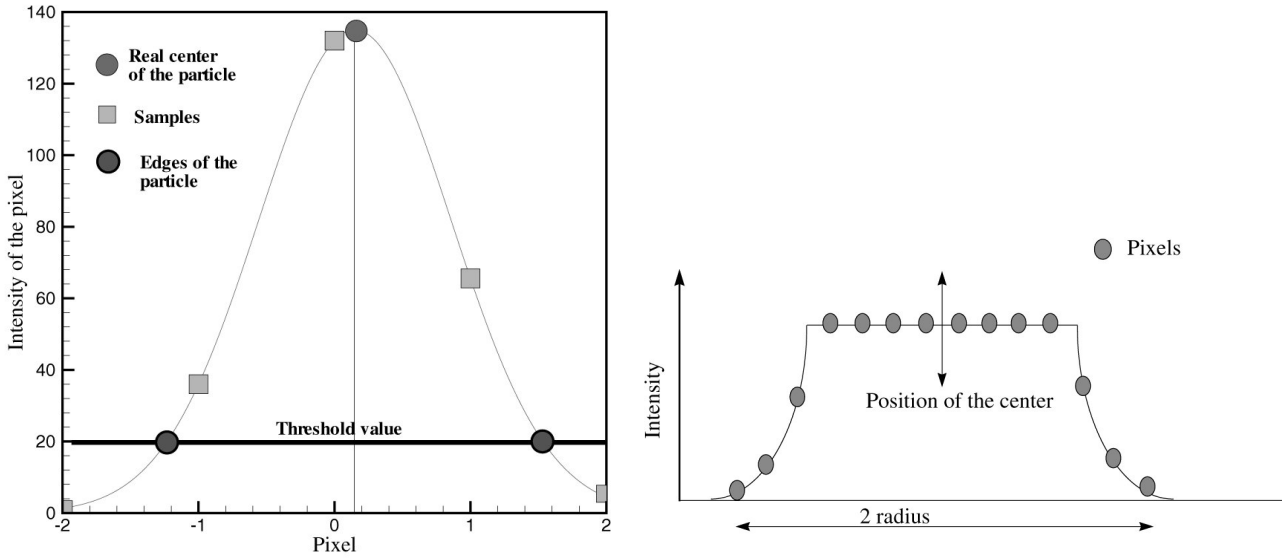

(a) Interpolation of the extremes

(b) Case of saturation of CCD sensors

Figure 3.2: Different approaches to get the size

3.4 Diffraction pattern

The last technique available is the one based on the Lorenz-Mie theory of light diffracted by droplets. If the camera is placed out-of-focus with respect to the laser sheet, the droplets show their diffraction pattern which typical example is shown on Figure 3.3. This work is part of the work performed by Giannoulis (1999).

The first task on such images is to isolate individual droplets in order to determine their own size. This can be done by using multiple filters, as presented in Figure 3.4. The principle is to first make a binary image by using a threshold. Afterwards, using dilation filter, it is possible to reform the droplet. The number of dilation operation depends on the size of the Alexander dark's band, which is responsible for creating two patterns in the binary image.

On such image, the ripple frequency is directly linked to the true size of the particle as described by the relation obtained by VanBeeck (1996), in case of second order diffraction.

$$F_{Ripple} = 0.01064 \frac{D_{Ripple}}{\lambda} \tag{3.1}$$

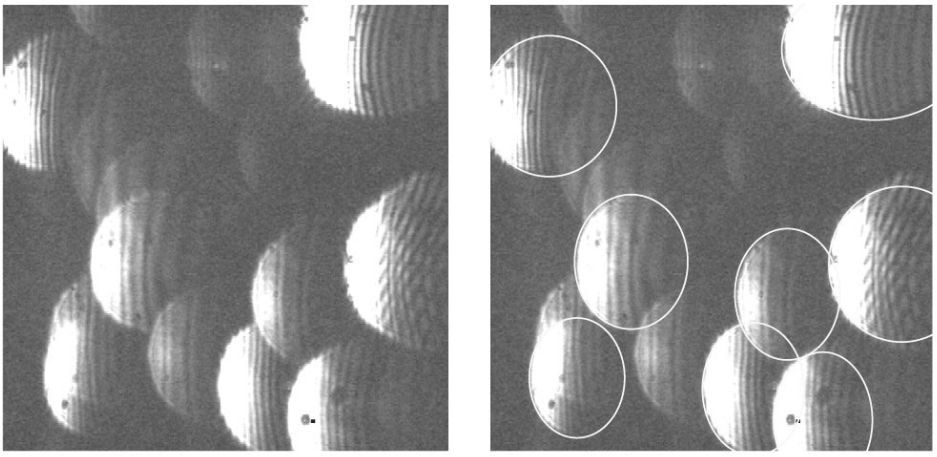

Figure 3.3: Selection of all droplets within an image

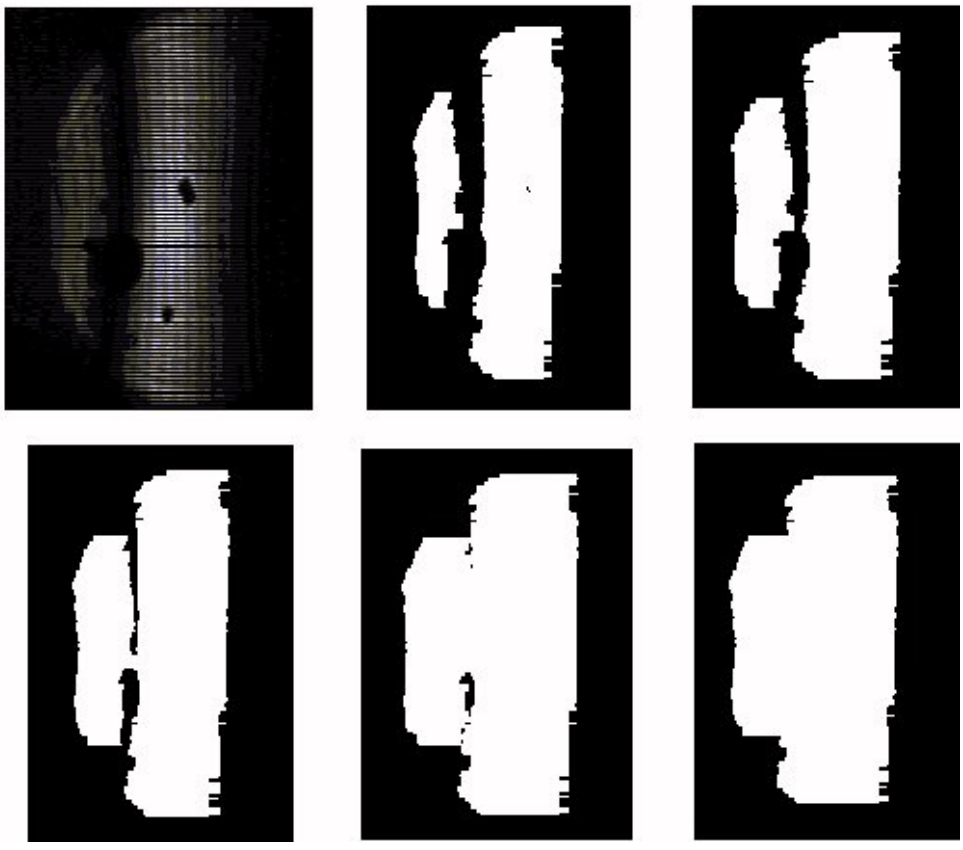

Figure 3.4: Steps to identify a droplet

where λ is the wavelength of the laser used. A full example is shown in Figure 3.5, together with the advantages found in taking a vertical sum of the pattern to compute the frequency and not only a horizontal profile, that may be spoiled by noise.

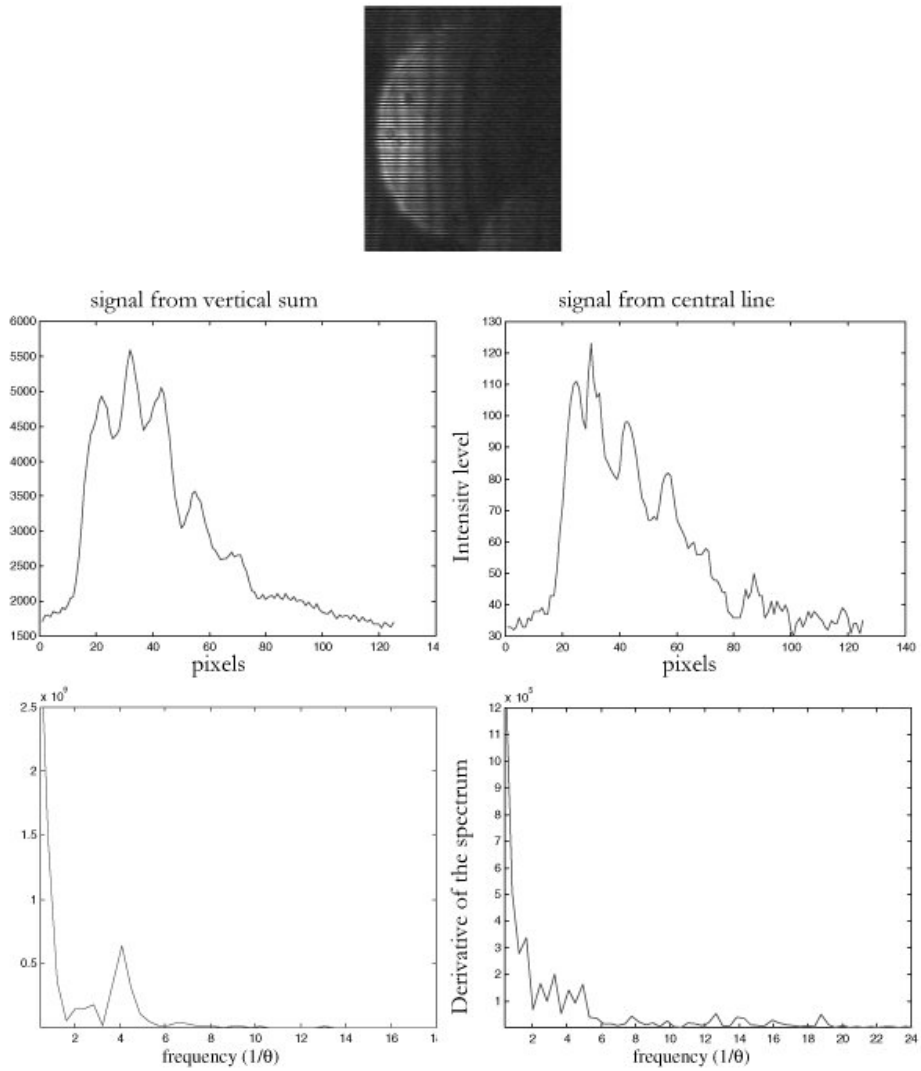

Figure 3.5: Determination of the ripple frequency for one droplet

Here also the main limitation arises for an increase of the void fraction. Recently, the use of a spatial filter to limit the diffraction pattern to very few lines has shown a clear benefit when applying this technique, as presented by Kobayashi *et al.* (2000). But, it is worth pointing out that placing the receiver at the rainbow angle (angle of the second order diffraction), one can also have the measurement of the temperature of the particles, postulating the law relating the changes of refractive index to the temperature is known. This comes to the Rainbow Interferometry theory, that is beyond the scope of this lecture. For further development of such techniques, see VanBeeck & Riethmuller (1996) and Zimmer *et al.* (2000).

Chapter 4

Particle tracking

This chapter aims at presenting the different possibilities to track individual particles and will shown their different ranges of applications.

4.1 Neural networks

A technique that is more and more developed to obtain the path of the particles, is to use a neural network which will optimize the cost functions in order to have the best global displacement. The main advantage of this technique is that no preliminary displacement is required to guide the tracking procedure. On the other hand, this requires usually a high computational time, as all the possible pairs are compared and the best one are kept. For more details about this kind of algorithms, one can refer to Ohmi & Li (1999) and Ohmi & Yoshida (2000).

4.2 Multiple exposed images

In this case, the principle is to use multiple exposed images to have the position of the particles at different time. A different time delay can also be imposed for a better determination of the trajectory, as depicted by Figure 4.1. For more details about this approach, see Cenedese (2000).

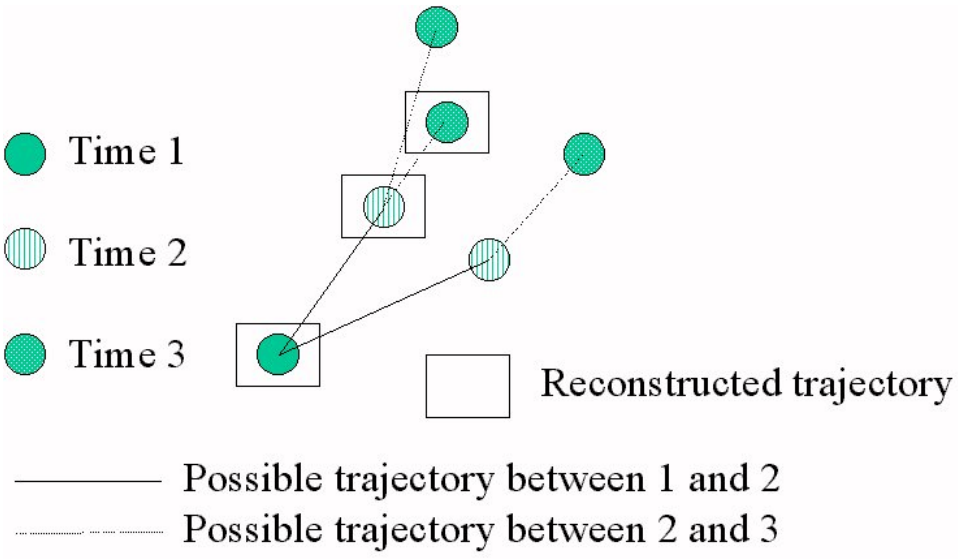

Figure 4.1: Principle of multi-exposure tracking

4.3 Super-resolution technique

This technique is an hybrid technique as requires a first treatment with correlations algorithms to have the displacement. Afterwards, the tracking algorithm takes benefit from this predicted displacement to limit the research area to a small zone on the second frame. The size of the research area can either be computed depending on local fluid velocity and gradient to estimate the zone. Another alternative is to fix a priori the maximum difference between the predicted displacement and the real one. The basic principle of this matching technique is sketched in Figure 4.2. This process is recursive as some pairing maybe removed for better associations. This is sketched in figure 4.3.

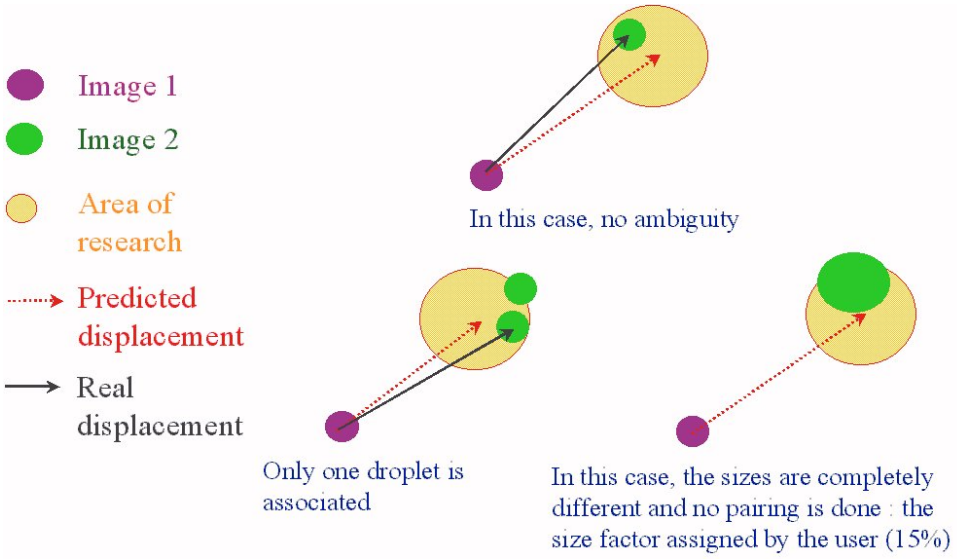

Figure 4.2: Principle of the super-resolution

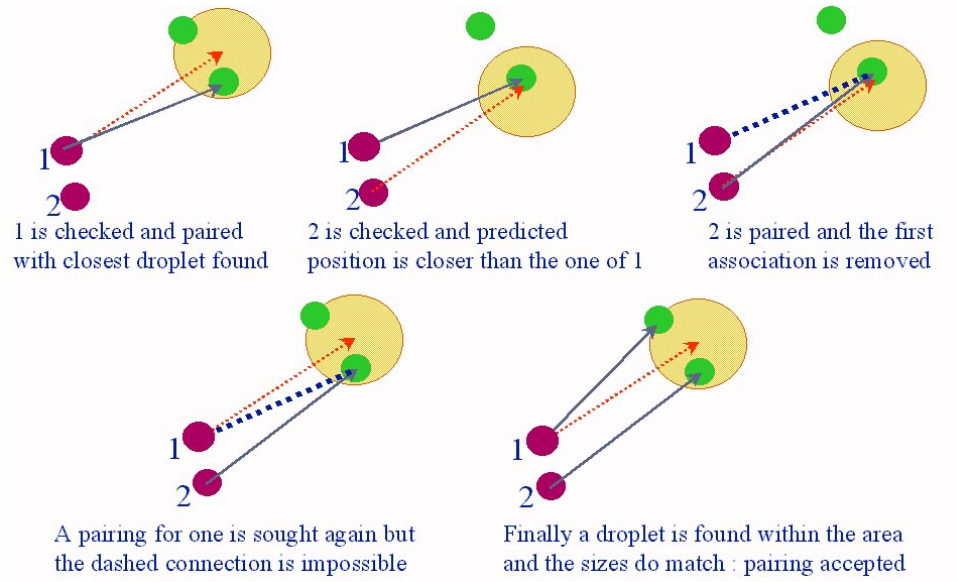

Figure 4.3: Iterative procedure for the matching process

4.4 Special treatment for two-phase flows

4.4.1 PTV-Sizing

In two-phase flows, one has to take advantage of the poly-dispersion of the sizes to enhance the reliability of the pairing process. For that purpose, when trying to build the connections between the particles on the first frame with those on the second one, the matching of size is imposed as well as the research area limitation, as presented in the case of single phase flow. The tolerance on the size matching depends on the accuracy expected on the size determination. Typical values of 15% are good to avoid losses of pairs, and to impose a good constraint. this limit will be discussed in the section 7.3.1.

4.4.2 Multi-layer PIV

An alternative to the masking technique is the decomposition of each image into layers of pixels having the same range of intensity. Afterwards each layer is correlated with the same layer one the second image and the mean displacement of each layer is found. As the intensity scattered by a particle is proportional to its diameter square, each layer represents a range of diameter. The absolute knowledge of the size is not possible to decide, as this should require a calibration to determine the incident light . As classical laser sheet exhibits a Gaussian profile, for each position the initial amount would be different. Nevertheless, applying this technique to real sprays showed very interesting results as presented by Ikeda *et al.* (1998). It could be shown that the smallest intensities follow the air flow, whereas big intensities respond less to the fluctuations of the fluid.

4.4.3 Streaked PIV-Sizing (SPIVS)

As discussed below, the hydrodynamic response of a particle highly depends on its size. therefore, continuous efforts are made to simultaneously get a two dimensional map of individual velocities and sizes of particles. A technique called Streaked PIV Sizing has been developed by Herpfer & Jeng (1995) for that purpose. The principle is to use two lasers; one continuous and a double-pulsed, as presented in Figure 4.4. The continuous laser has two main interests. The first is to illuminate the particle in order to have a streak of the path. The second purpose is to enable the size measurement by integrating the total amount of light scattered by the particle. This second feature requires a calibrating operation, as discussed above, making its use difficult. The sizing ability has been discussed by Herpfer *et al.* (1995) showing a similarity between the distribution obtained by PDA (Phase Doppler Anemometer) and the one by SPIVS, when supposing an equal mean diameter, as SPIVS is only able to give relative size distribution. Concerning the measurement of the velocity, the use of the double-pulsed laser is required. It creates two big spots for each particle. Afterwards, knowing the time delay between the two pulses and the displacement of the particle along its streak gives the velocity. Measurements reported were comparable with PDA measurements.

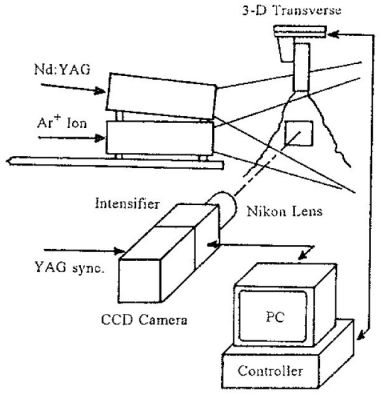

Figure 4.4: Experimental requirements for applying SPIVS as presented by Herpfer *et al.* (1995)

4.5 Interpolation on structured grid

Whatever the algorithm used, at the end of the tracking procedure, one ends with local displacement of particles. But, what is usually required for comparisons purpose is the velocity on a structured grid. This requires an interpolation from the scattered displacement to a grid. It has been shown by Agui & Jiménez (1987), that the best solution is the use of an Adaptive Gaussian Window.

The formulation of the adaptive Gaussian window scheme is given by equation 4.1.

$$f = \exp\left(-\frac{x^2 + y^2}{h^2}\right) \tag{4.1}$$

4.6 Validation procedure

As described by Westerweel (1994), a spurious vector is visually recognized as a vector exhibiting an "unexpectedly large" deviation with respect to nearby vector. In PIV experiments, it is very important to interpolate those bad vectors, as the final result has to be displayed uniformly. In PTV, as the output is unstructured, there is no need for interpolating bad vectors. But this does not prevent from detecting and erasing them. Like in PIV, the local deviation with respect to nearby displacement is computed. Here again, there should be a dynamical threshold to remove the bad vectors, as the deviation must be a decreasing function of the distance between the vector sought and the others. An illustration of such a procedure is shown in Figure 4.5.

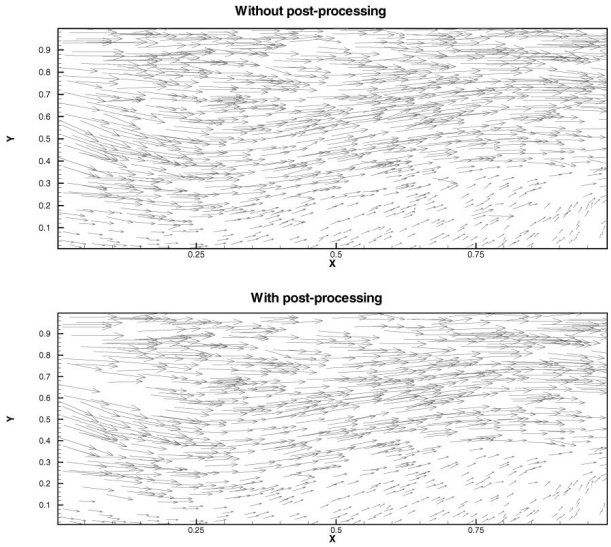

Figure 4.5: Use of post-processing to remove bad pairing

Chapter 5

Validation on synthetic images

To evaluate the validity of the developed softwares, one can use synthetic images. The advantage of the synthetic images is that the displacement is known and different parameters as maximum gradient or seeding density can be easily controlled. All the images here are taken from the Standard PIV project, hosted by www.vsj.or.jp/piv and developed by Okamoto *et al.* (1997).

5.1 Shear wall flow

Together with a set of images, the reference flow field is provided (see Figure 5.2(a)). It is possible to simulate different densities, as shown in figure 5.1 showing together a high seeded density image (Figure 5.1(a)) and a low one (see Figure 5.1(b)).

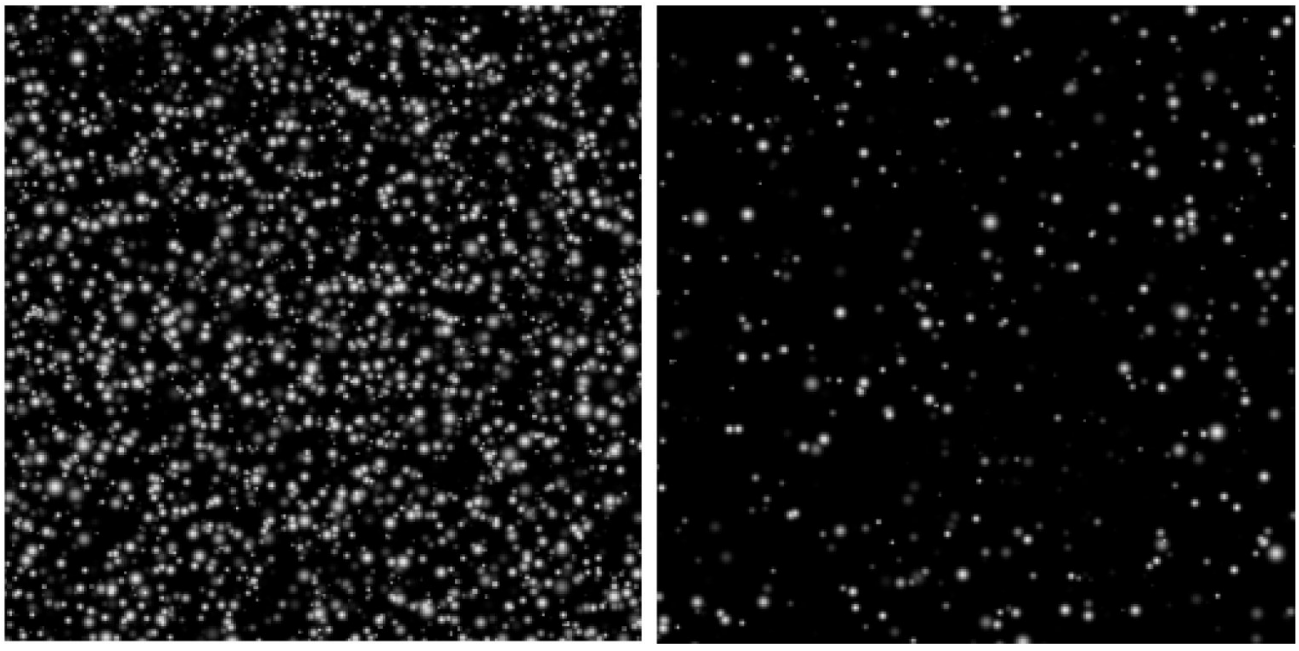

(a) Reference flow field

(b) Results of the tracking algorithm

Figure 5.1: Application of tracking on synthetic images

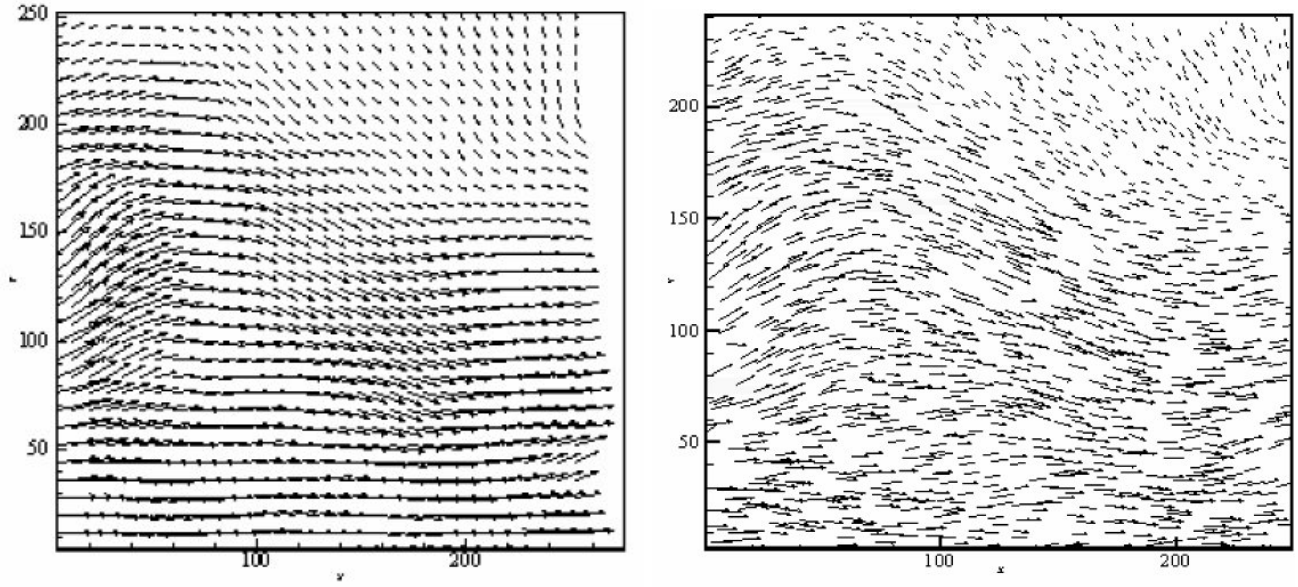

(a) Reference flow field

(b) Results of the tracking algorithm

Figure 5.2: Application of tracking on synthetic images

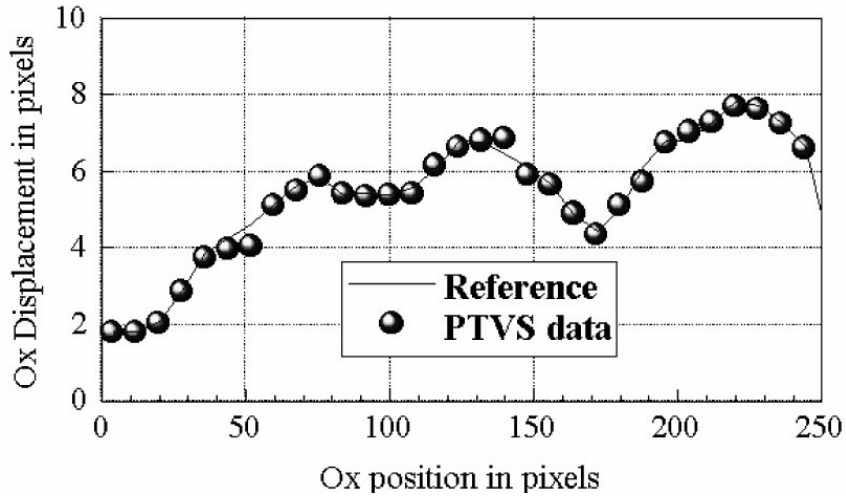

Figure 5.3: Velocity profiles taken at Y=100

5.1.1 Influence of density

As the density can be changed, it is possible to study the effect of the density on the final results obtained by PTV. The Table 5.1 show the influence of the density for an image of 256 by 256 with a mean size of 4 pixels per particle.

Number of particles	Number tracked	Success rate
20	15	100
500	450	95
1000	955	90
2000	1900	85

Table 5.1: Different configurations of the synthetic images

5.1.2 Influence of the size of the particles

As the principle of PTV is to track each individual particles, the accuracy achieved will highly depends on the one obtained in determining the center of each particle. The identification is done using a 3 point Gaussian scheme. It has been showed that using best-fit Gaussian does not really improve the accuracy, but is more time consuming (Zimmer (2000) and Marxen *et al.* (2000)).

Mean size (pixel)	Dispersion	Typical error
1	1	0.25
2	1	0.2
3	1	0.13
4	1	0.1
5	1	0.07

Table 5.2: Quantification of the influence of the tracers' size

5.2 Free jet

Another series of images provided are simulating a free jet. The interest of this series is to provide a time series composed by 144 successive images. This is important to validate the tracking procedure within consecutive frames, as used after in section 6.2. Its the series labeled 301.

5.2.1 Presentation of the flow

The simulated conditions of the series of images is wrapped up in table 5.3.

Image size (pixel)	256 x 256
Area (cm)	4 x 4
Laser thickness (mm)	2
Interval (ms)	5
Max. velocity (pixel / interval)	10
Max. out-of-plane velocity (%)	15

Table 5.3: Conditions for the generation of the synthetic series

A typical velocity field is given in Figure 5.4(a).

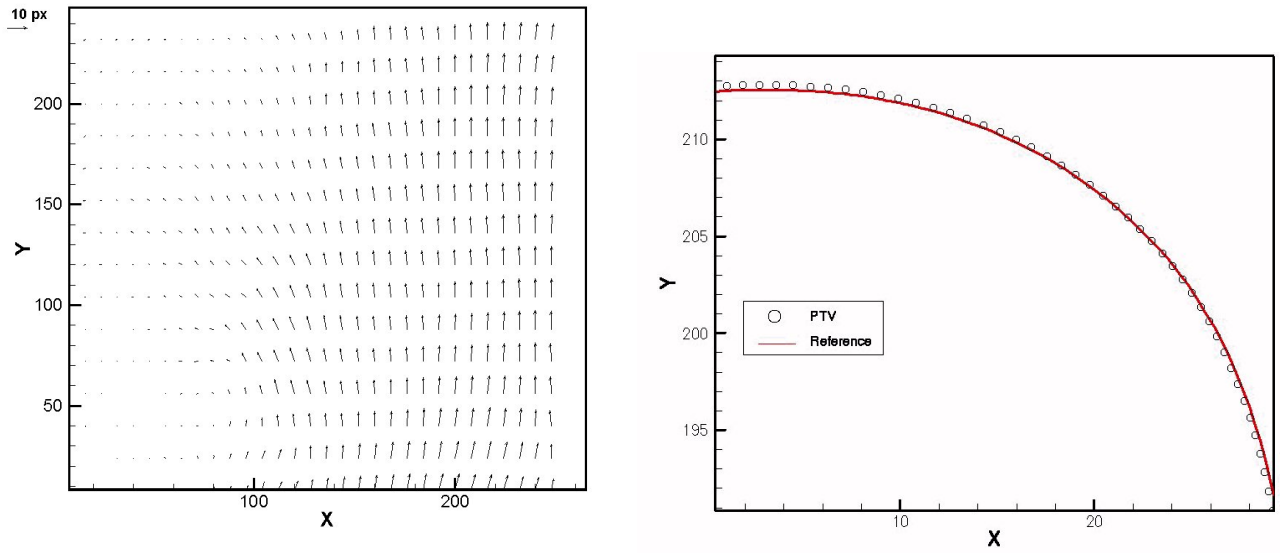

(a) Velocity profiles taken at Y=100

(b) Comparison between measured trajectory and imposed one

Figure 5.4: Application of tracking series on synthetic images

5.2.2 Comparisons between the trajectories

Together with the images, the position of all the particles are provided with an identification number. This allows to track a particle within all the images and to compare the trajectory with the one obtained by applying PTV to the series of images.

A typical comparison is shown in figure 5.4(b), where we can see the measured displacement represented by the circles and the imposed one, depicted by the continuous line. The error made is the error resulting from the exact location of the center of the particle.

Chapter 6

Validation on real images

6.1 Combustion flame from PIVNET image

6.1.1 Presentation of the image

Recently, there is an effort to provide common database of images coming from real experiments. Among the different images, there is the one coming from a combustion flame, as presented in Figure 6.1.

Figure 6.1: Image from a combustion flame

6.1.2 Typical results

The raw PTV results are displayed in Figure 6.2. As can be noticed, displacement are not found everywhere in the image, but only in the seeded regions. The inner region having a high density is also well captured by the PTV processing. This illustrates the fact that the PTV can deal with high seeding density, as long as individual particles can be found on the image.

6.1.3 Comparisons with PIV results

Interpolating the scattered results obtained on the PTV image, one is able to compare with the results provided by PIV analysis. Taking a horizontal profile at Y = 200 pixels, and plotting simultaneously the PIV and PTV

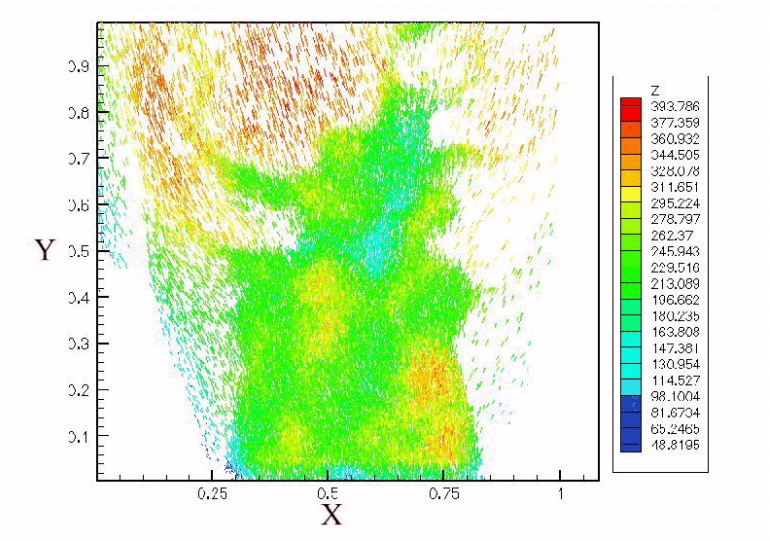

Figure 6.2: Results of the tracking

results (Figure 6.3), one see that in the edges, PIV founds a displacement, but that can not be found by PTV. The reason for the non displacement of the PTV result is that there is no particle in this region. Therefore, the PIV results are not based upon displacement of particles, nut maybe a noisy pattern. What is also interested to see is that the gradients of velocity found on the edges are the same for the two techniques.

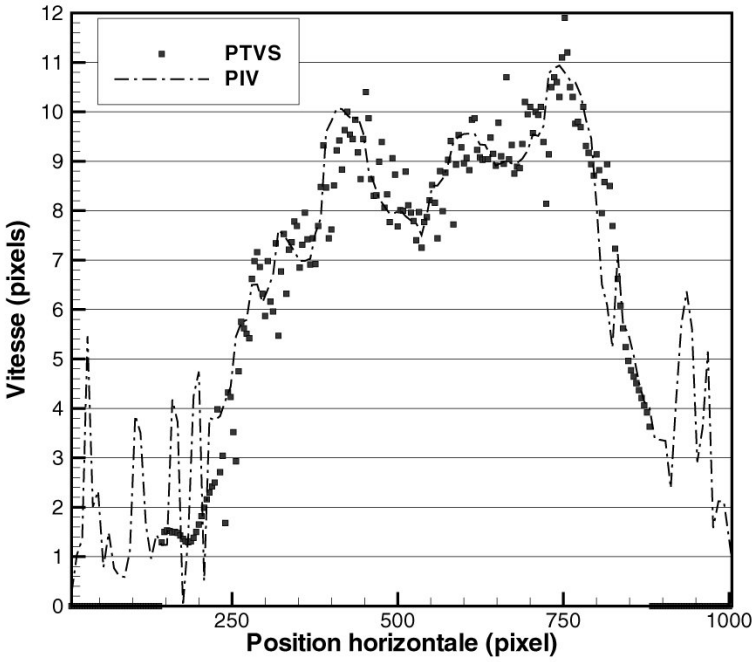

Figure 6.3: Profiles obtained by PTV and PIV

6.2 Tracking within lungs bifurcation

6.2.1 Presentation of the setup

This work has been carried out in VKI by Ramuzat *et al.* (1999) and Ramuzat & Riethmuller (2000). This introduction is to illustrate the context of the present study and the importance of tracking procedure. In many biological problems, fluid dynamics plays an important role such as, for example, airflow in the lung, blood flow in the circulatory system, flows in the kidney, etc. In our environment, asthmatic problems or chronic pulmonary disease due to pollution effects become more and more important. To identify the factors, which may be contributing to breathing disturbances and to the contribution of pollution effect on the alterations in breath patterns, a better understanding of the human pulmonary system is needed. As a result, fields to be investigated are mostly flows in lung under high breathing frequency and aerosol deposition in lungs in bifurcations under unsteady conditions. The respiration pattern has to be better understood and investigated to have the possibility to get the best appropriate palliative treatment. Most of the medical treatments are based on aerosol deposition in the bronchial tree.
The lung is a complex network of successive bifurcations. The airways, from the trachea to the alveolar zone, divide by dichotomy and become shorter and narrower as they penetrate deeper into the lung. As a result, in vivo investigations of pulmonary flows are not possible, and in vitro experiments in models have to be performed. A complete description of steady flow in a single 3D bifurcation has been previously performed at VKI by experimental and numerical modeling. As a result of this study, it has been shown that the first bifurcation influences the flow in the second and in the third bifurcation when the length of the second one is not sufficiently long.
To extend the investigations on a system of three generations, this study has been carried out on a 3D network of bifurcations. To experimentally investigate flows within three-dimensional multiple bifurcations, a three-dimensional model has been built with an innovative casting technique. This technique is using an alloy with a low melting point and a mixture of silicone and curing agent. The particularity of the silicone is its transparency, which allows a high quality optical access. This 3D experimental model of a multiple bifurcation has been scaled-up from the physiological data and the geometric characteristics of each bifurcation have been strictly preserved. The scaled experimental model respects the dynamic similarity with the two main non-dimensional parameters of this study, the Reynolds and Womersley numbers. The choice of the pulmonary zone to be studied is the laminar flow zone of the conducting part where the Reynolds is ranging between 200 and 1000. The Reynolds number is based on the width and on the mean velocity in the parent branch.
The Particle Image Velocimetry technique has been used to measure the whole velocity flow field, for different flow conditions. For that purpose, the technique has been modified to particularly suit to low speed flows studies. This method makes use of a continuous 4 Watts laser and the acquisition of the PIV pictures are directly performed with a MIRO card, which allows an acquisition of up to 1000 successive images. Unsteady measurements have been performed with a piston movement ensuring a sinusoidal flow rate. The variable flow rate is controlled by a piston system. The resulting unsteady flow can be varied substantially in amplitude and frequency, this covering a wide range of Reynolds and Womersley numbers. The mean velocity of the flow was fixed to zero. The displacement of the pistons was varying as $\sin \omega t$.

6.2.2 PIV results

The PIV results give the instantaneous velocity field in function of the time, as it is time resolved PIV . Having this instantaneous velocity, it is possible to track a virtual particle (neutrally buoyant) within all the successive frames. This will give the different positions it has versus the time. This is done for a frequency of 0.2Hz and a maximum Reynolds number of 400. Depending on the starting point, the amplitude of the movement will differ a lot, being quite big in the main tube and a bit smaller in the two daughters branches. To really assess this approach, PTV algorithms are used to track individual particles.

6.2.3 Tracking

Applying super-resolution PTV, the displacement of real particles is computed at each time step. From those instantaneous displacement, the real trajectory of a particle can be reconstructed, as the same frame is used two times, one has target frame and then as initial frame for the tracking procedure. Afterwards, a small program, reading the tracking results, can reconstruct the displacement. The important requirements to apply such a technique is that the particles remain at least for a complete cycle in the image, therefore 3D effects should be

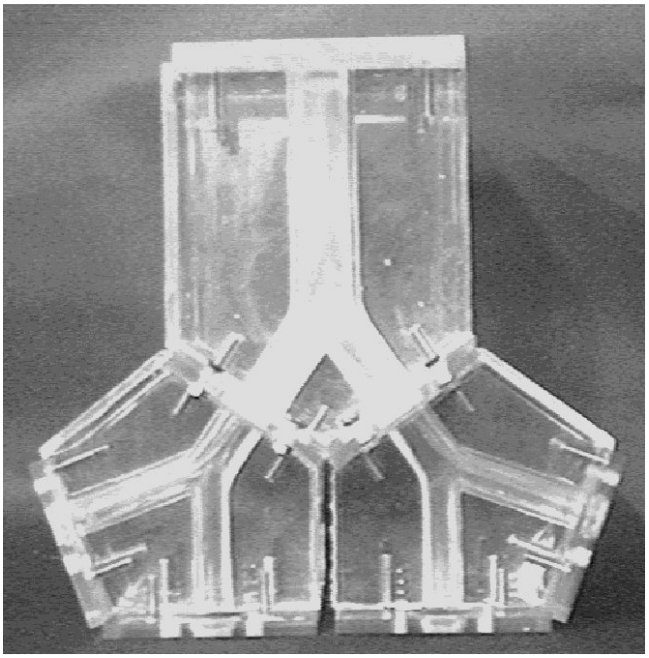

Figure 6.4: View of the lungs bifurcation's model

quite small, or a bigger laser sheet has to be used.

6.2.4 Comparisons with PIV predicted displacement

Having the PIV results, it is possible to integrate the displacement that should have a neutrally buoyant particle and hence to determine its path.
To validate this procedure, the only possibility is to perform tracking for the same conditions and reporting the experimental path together with the theoretical ones. One comparison between the real trajectory of a particle and the one resulting from the integration of the velocity vector is displayed on figure 6.5(a), where the points represent the experimental positions and the line the numerical one. One can see a good agreement in the inflection point for a time code of 176.
The result obtained from the integration of the PIV velocity field shows a phenomenon called Steady Streaming Displacement; The Steady Streaming Displacement concerns the local deposition sites of inhaled particles and aids in gas-exchange. This phenomenon is related to the displacement near the bifurcation of a fluid element during a complete period. The initial location of the fluid element has an effect on this flow phenomenon. In fact, when, at the beginning of the expiration, the particles suspended in the flow are far from the bifurcation, they are less affected by the bifurcation effect. The displacement of the fluid element after one period of oscillation decreases when the initial position of the particle is far off the bifurcation carina. This phenomenon is of interest for High Frequency Ventilation (HFV) and its potential clinical use during surgery and in the intensive care setting.

6.3 Conclusions

The PTV approach using super-resolution principle is a diagnostic tool that can be used in different conditions. The limitation in terms of seeding density are becoming less strong with an increase of computers' efficiency. As far as continuous trajectories are concerned, even an algorithm based on double exposure images can be used to provide the evolution of the position versus time. The study of lungs bifurcations shows that to have the trajectory of particles, PTV is more suited than interpolating PIV displacement fields, in the case of strong gradients. The reason is the limitation of the windows size that must remain big enough to have 10 particles, therefore, the gradients can not be well caught. As the displacements are quite small,

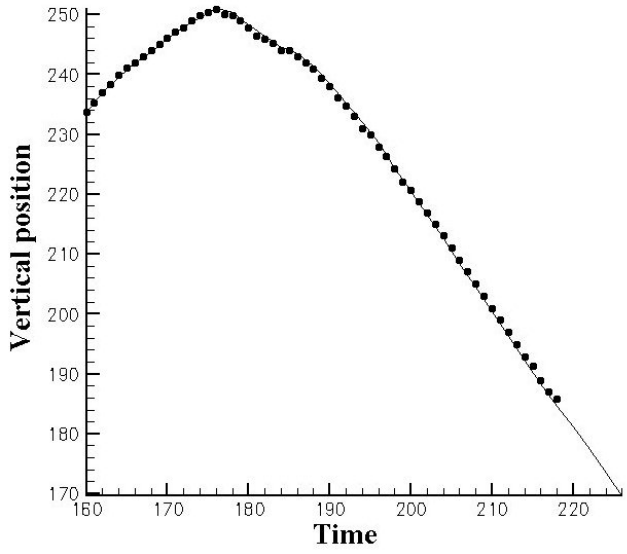

(a) Comparison between real trajectory and simulated one in the main branch

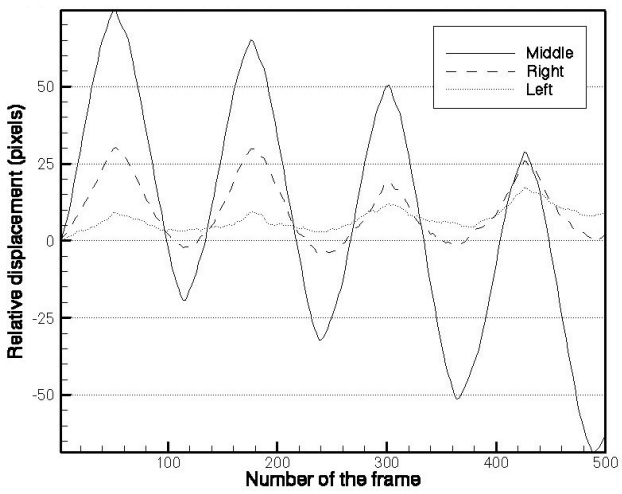

(b) Comparison between real trajectory and simulated one in a daughter branch

Figure 6.5: Integration of velocity field

Chapter 7

Validation with sprays only

To validate the developed technique, a series of experiments have been carried out on single spray and mixing of sprays. In those experiments, only water droplets are used. The air is not seeded with oil particles. Therefore, the only results obtained will be the size and the velocity of the droplets. Comparisons with PDA measurement will show the capability of the sizing feature of the PTVS.

7.1 Sizing ability

The detection algorithm used is the one based on peaks detection (2.3). The sizing algorithm chosen in the present case is the one based on the limits of the Gaussian function (3.3). To see its efficiency , a comparison is performed with results obtained by Phase Doppler anemometer Bachalo & Houser (1984). The PDA gives the mean size of droplets in one single point. There exists different typical diameter in sprays that can be measured. Among them, there is the Sauter diameter that is defined as

$$D_{32} = \frac{\sum_{i=1}^{i=nb} d_i^3}{\sum_{i=1}^{i=nb} d_i^2} \tag{7.1}$$

It can be interpreted as the diameter that defines the ratio between the buoyancy force (αD^3) and the inertial one (αD^2). Furthermore, there is some typical laws in sprays based on this diameter. Therefore, the assessment of the PTVS will be based on this diameter. It is worth noting that the two techniques measure

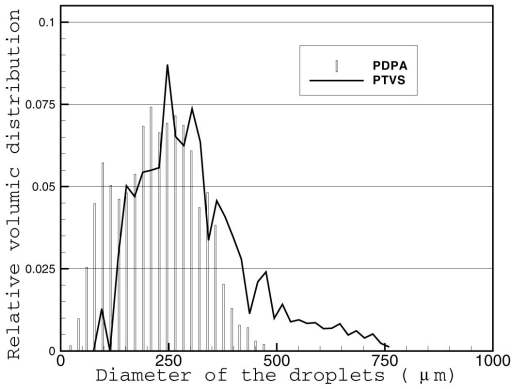

Figure 7.1: PTVS-PDA comparison in the core

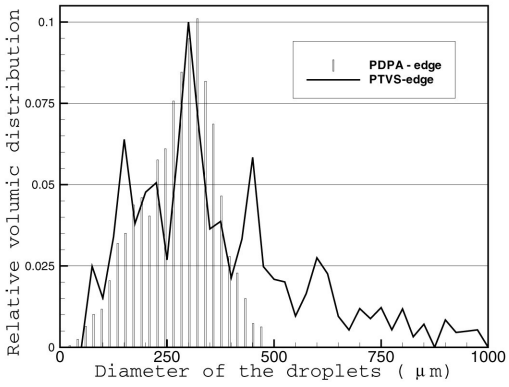

Figure 7.2: PTVS-PDA comparison in the edge

an increase of the diameters as the measurement is done towards the edge of the spray. This is consistent with the theory and is due to the fact that momentum exchange between the droplets and the surrounding gas will tend to entrain gas within the spray. This entrainment will affect mainly the smallest droplet, that have a lower momentum than the bigger one. The PDA technique is limited to spherical object, whereas PTVS is not. Measuring the diameter in the two mean directions can lead to an estimation of the sphericity of the droplet.

Hence, if one only wants spherical droplet, one can limit the difference between the two measured diameters. On the other hand, one can size even non-spherical droplets. The problems of non-sphericity is however usually

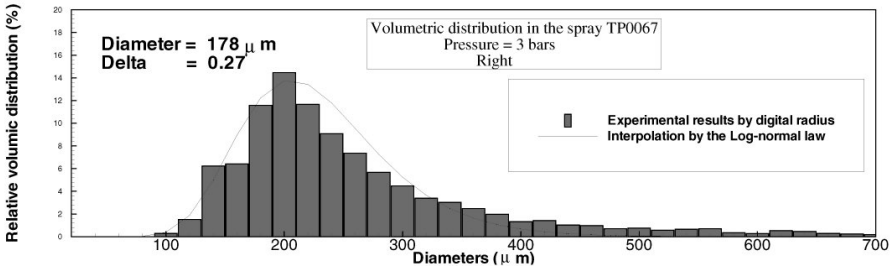

Figure 7.3: Comparison between PTVS and Log-normal law

present only for big droplet. The difference that can be observed for the big diameters come also from the fact that the dynamic range of the PDA is a bit slower than the one of PTVS. Another way to asses the sizing measurement is the comparison with a standard distribution occurring in liquid sprays. The one that is used in the present study is the Log-normal law (Prétrel (1997)) that can be represented by :

$$f(d_i) = \frac{1}{\sqrt{2\Pi}\xi\overline{d}} exp\left[-\frac{1}{2}\left(\frac{Ln\left(\frac{d_i}{\overline{d}}\right)}{\xi}\right)\right]^2 \tag{7.2}$$

where the two parameters $\overline{d}$ and ξ are the mean logarithmic diameter $Ln(\overline{d}) = \sum_i \frac{n_i}{n_{tot}} Ln(d_i)$ and the dispersion coefficient $\xi = \left[\sum_i \frac{n_i}{n_{tot}} \left[Ln\left(\frac{d_i}{\overline{d}}\right)\right]^2\right]^{0.5}$. The number of droplets belonging to class i is n_i whereas n_{tot} is the total number of droplets in the sample. A typical comparison with PTVS measurement is displayed on Figure 7.3. This emphasizes the reliable measurement of a size distribution by PTVS.

7.2 Velocimetry

Once the center of the droplet as well as its size are found, the tracking procedure can be used in order to measure the velocity of individual droplets.

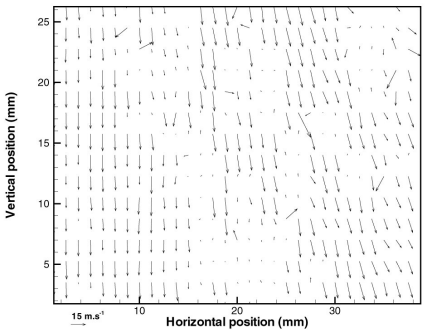

Figure 7.4: Classic PIV results in one spray

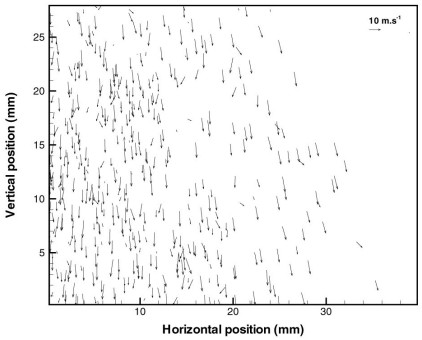

Figure 7.5: PTV results for one spray

As explained in Chapter 4, the first step is to compute a mean displacement. This is obtained using a cross-correlation technique(Scarano & Riethmuller (1999)). A typical example is shown on Figure 7.4. This initial velocity field is used afterwards to track each individual droplets within the two frames. We can distinguish two main regions in the PIV results. The first one is a simple downwards movement (for $X < 20mm$). The other part of the image is composed by velocity vectors having a given horizontal velocity. On the tracking results (figure 7.5), we understand better the two regions obtained previously by the PIV algorithm. As the measurements are performed in the vicinity of the edge of the spray, the outer droplets have still this horizontal velocity, whereas in the core of the spray, this component tends to disappear. It is important to understand

that each vector is the displacement of a specific droplet with its own size. It is also important to notice that PIV gives results even in regions where no droplets are on the image. When comparing the magnitude of the velocity obtained by PDA and PTVS (see Table 7.1), one can see a good agreement between the two techniques. The difference comes from the fact that it is very difficult to ensure the reproduction of the same conditions for the spray.

Horizontal position (mm)	Velocity with PDA ($m.s^{-1}$)	Velocity with PTVS ($m.s^{-1}$)
0	6.2	5.8
20	4.8	4.8

Table 7.1: Different configurations of the synthetic images

7.3 Mixing of sprays

7.3.1 Identical sprays

A challenging experiment will be to investigate the mixing of two identical sprays, and to see if it is possible to retrieve the origin of the droplet. For such a purpose, two identical sprays are used under the same feeding

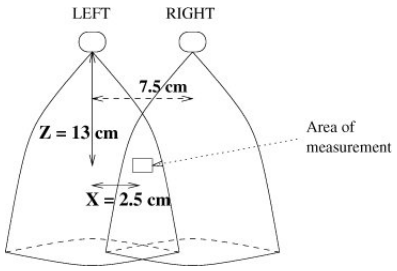

Figure 7.6: Principle of the mixing experiment

pressure. Therefore two identical distributions are to be expected. But in the region of interest, the droplets issued form the right nozzle will have a negative horizontal velocity, whereas the other one will have an opposite displacement. If the mixing process is not fully achieved, it should be still possible to distinguish two families of droplets by PTVS. Those PIV results do not help in understanding the internal structure of the spray,

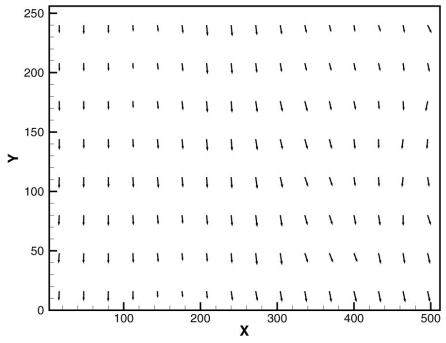

Figure 7.7: PIV results for inter-penetrating sprays

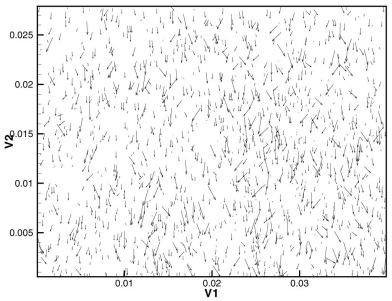

Figure 7.8: PTV results for inter-penetrating sprays

neither in understanding the mixing process. They can just provide the mean displacement of a region, whether there are droplets in this region or not. But, when using the PTVS processing technique, one can measure individual displacement of droplets. Such a treatment has been applied to obtain a two-dimensional map of an instantaneous field of droplets, as depicted on Figure 7.8. To emphasize the need of the sizing-factor, a horizontal profile is taken when computing the velocity field with a sizing factor of 15% and another one of

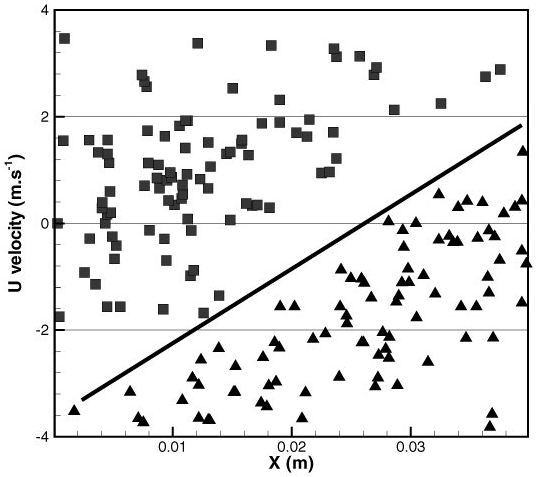

Figure 7.9: PTVS results for a sizing factor of 15

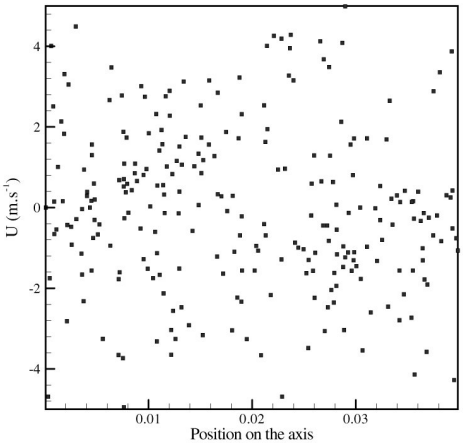

Figure 7.10: PTVS results for a sizing-factor of 1000

1000%. One can see on Figure 7.9 that two categories of droplets can still be distinguished, whereas on Figure 7.10 it is hardly possible to see the two families.

Droplets emerging from the spray of the right will have a negative horizontal velocity. This velocity will increase when taking the measurement far from the center because of the angle of ejection of the spray. The reason for that behavior is that for the height investigated ($z = 12cm$), the initial velocities of the biggest droplets are not really affected by the gravity and by the entrainment of air within the spray.

7.3.2 Different sprays

In industrial application when mitigation of hazardous release is concerned, one may combine two different sprays. the following experiments is based on this principle and a spray having a bigger momentum, as right's spray is used. The spray used is another flat fan spray ($TP400005$ from $SprayingSystems$). Its flow-number is $6.1 \pm 0.210^{-5} kg.s^{-1}.Pa^{-1/2}$. The measurements were performed at 30cm from the nozzles and the origin of the X-axis was chosen as being in the centerline of the spray of the left. The results are given in terms of mean Sauter diameter. On Figure 7.11, one can see an increase of this diameter. Furthermore, one can see the influence of the second spray (labeled right). It controls the mixing process, and this is consistent with the fact that it has a higher momentum. Those results show the ability of the presented PTVS to size droplets within sprays.

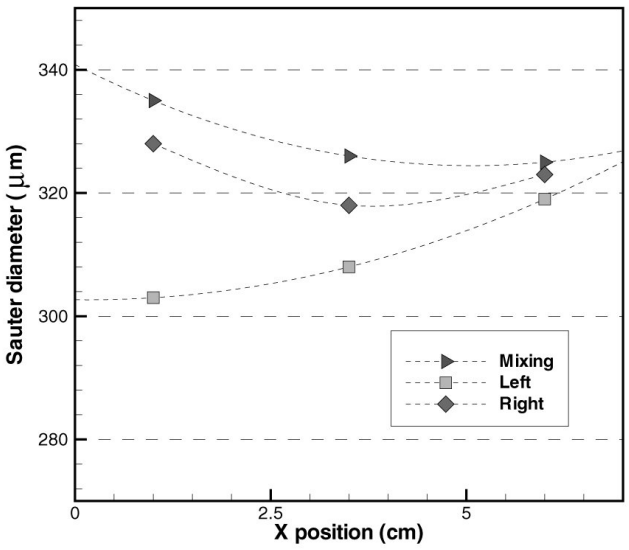

Figure 7.11: Mixing different sprays : size distribution

Chapter 8

Validation on two-phase flows

In many experiments, the main goal sought is to have simultaneously the displacement of the particulate phase and the carrier phase. Therefore, on images, one may have together the seeding particles and the discrete phase. As the sizes are different, it is possible to distinguish them. In the present part, two applications are presented using water sprays discharging in air.

8.1 Mixing layer

This work has been carried out at the von Karman Institute in the Environmental and Applied Fluid dynamics department by Suda (2000).

8.1.1 Presentation of the experiments

A vertically placed twin-jet wind tunnel having 6:1 nozzle contraction ratio and jet exit cross section area of 200x300 mm, is divided into two 100x300 mm rectangular jets by a splitter plate /SP/. Each of the section has is own air supply and smoke generator. The basic notations and coordinates of the downward plane mixing layer flows were used. The origin of the Cartesian coordinates located at the center of the splitter plate which has an edge thickness of a tenth of mm and the opening angle of the SP is about 1 degree. The streamwise direction originated from the trailing edge of the splitter plate is the x coordinate axis, while y axis, starting from the trailing edge normal to the plate, is the transversal direction. The spanwise direction is noted as the z axis. The ultrasonic atomization type spray nozzle was placed into the high-speed part stagnation chamber, downstream of screens, honeycombs and the smoke injection unit. Special care was taken of spray positioning, hence droplet deposition on the splitter plate surface was successfully avoided. The available test section of free mixing layer flow was up to x 650 mm downstream of the twin-jet exit.

8.1.2 Preliminary results

Visualization

Before presenting quantitative results, images to show the physical behavior of the mixing layer are plotted. It is worth noting that those images are not processed to have the velocity measurements, as the seeding conditions are not adequate for such a purpose. The two tunnels are working but only the lower velocity is seeded, whereas the droplets are injected in the high speed part of the facility.

Mean velocity obtained by PIV

All the measurements are taken in the spanwise mid-plane of the test section, as shown in Figure 8.3. The first steps towards the measurement of the two phases is the use of classic cross-correlation technique, by applying windows distortion together with an adaptive size, as presented by Scarano & Riethmuller (1999).

A series of mean velocity as well as instantaneous velocity field can be computed, and typical examples are shown on Figure 8.4

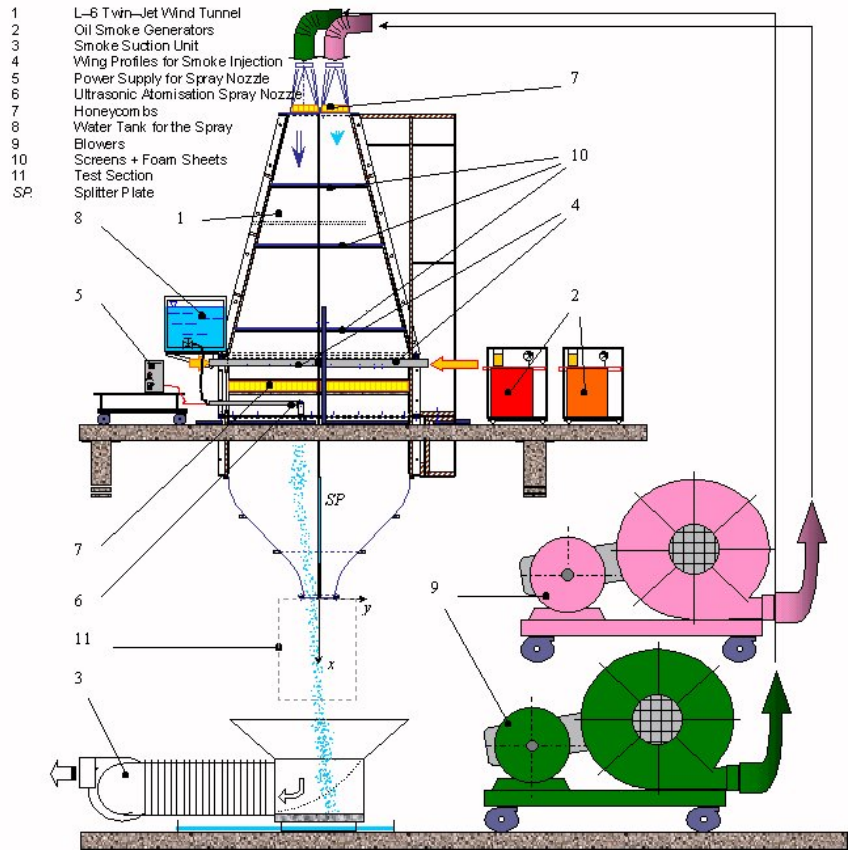

Figure 8.1: Experimental device to create the shear layer

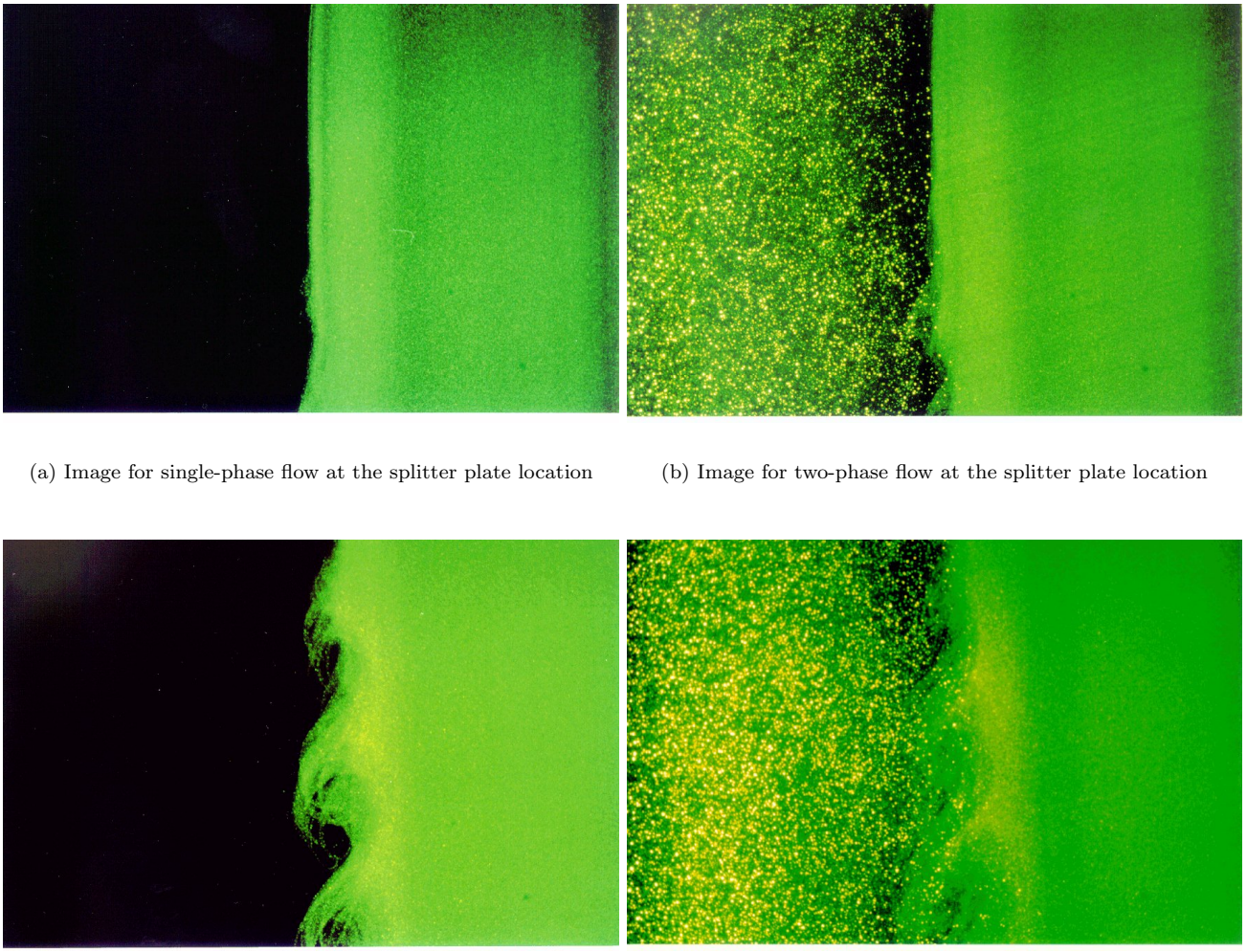

(a) Image for single-phase flow at the splitter plate location

(b) Image for two-phase flow at the splitter plate location

(c) Image for single-phase flow at 100mm from the splitter plate

(d) Image for two-phase flow at 100mm from the splitter plate

Figure 8.2: Visualization of the flow conditions

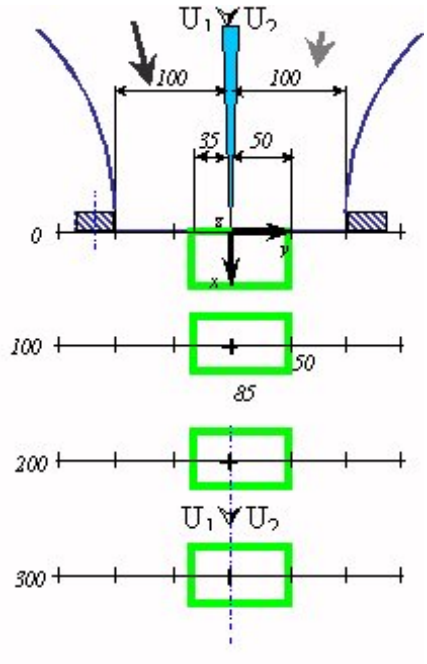

Figure 8.3: Localisation of the experimental windows

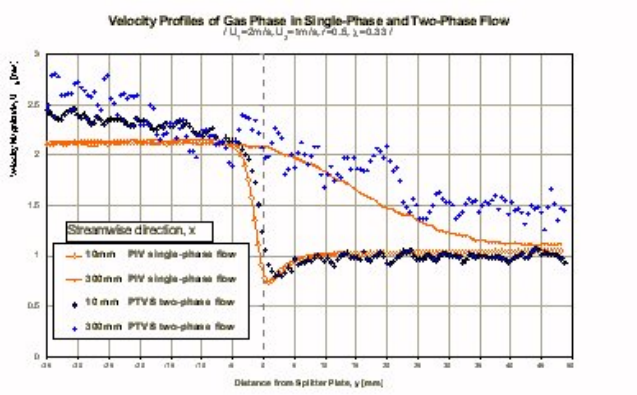

(a) Changes in the mean velocity due to the droplets

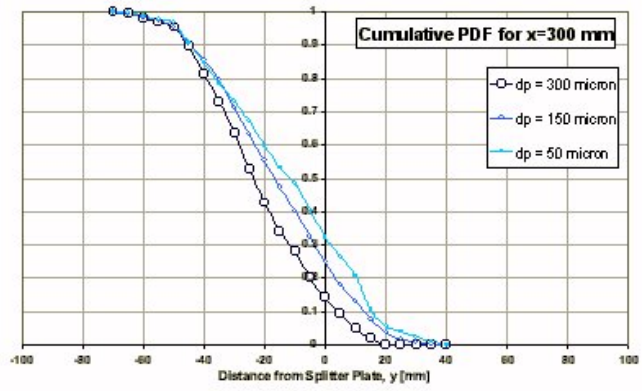

(b) Probability density function of the droplets at 300mm from the splitter plate

Figure 8.4: Typical images for the two-phase flow conditions

8.1.3 Two-phase flows measurements

Typical images

When injecting the droplets, there must be a special treatment, in order to account for the different velocities, depending on the different sizes of the droplets. As shown on figure 8.5, there are droplets together with seeding particles on the image.

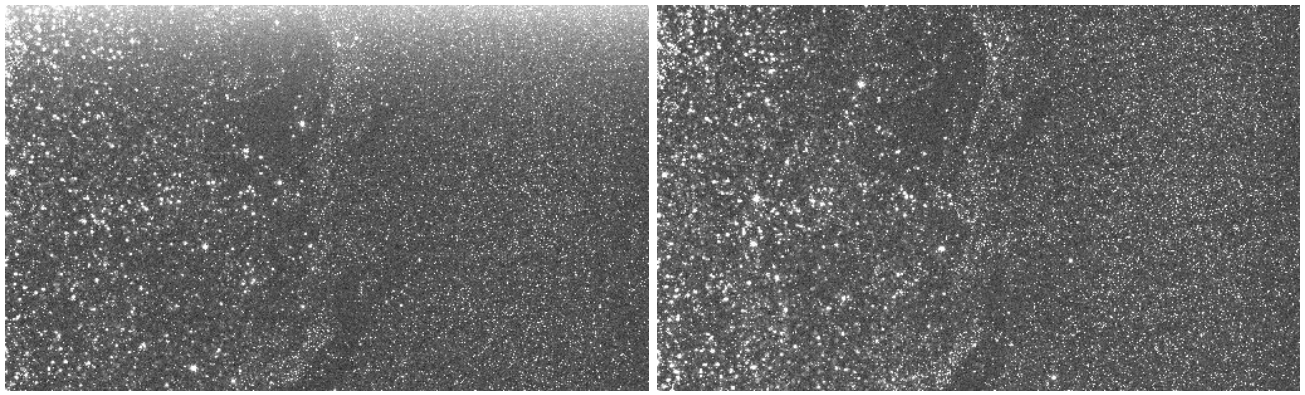

(a) First image use for tracking

(b) Second image use for tracking

Figure 8.5: Typical images for the two-phase flow conditions

Results

The comparison between the single phase case and the two-phase flow conditions indicates that the discharge of droplets in the higher velocity part introduces a small over-velocity due to momentum exchange between the fluid and the droplets. This increasing initial velocity can be seen on Figure 8.4(a). When performing measurements at 300mm from the splitter plate, one can see that the droplets have a bigger influence on the carrier phase. As expected, there is still an increase of the velocity, especially for a location of 20 mm with respect to the splitter plate. This is due to the fact that when looking at the probability density function of the droplets along the streamlines, some of the big droplets are located at such a position. Because of their settling velocity, they tend to increase the movement of the surrounding fluid.

8.1.4 Turbulent changes

The final purpose of this study is the measurement of either enhancement and dissipation of turbulence due to the droplets. This is possible with the present technique as the fluid quantities are measurement with and without droplets. The results are summarized in Figure 8.6 and compared with reference cases as presented by Gore & Crowe (1989). The size of the dots are function of the droplets' diameter. A full explanation is given in Suda *et al.* (2001).

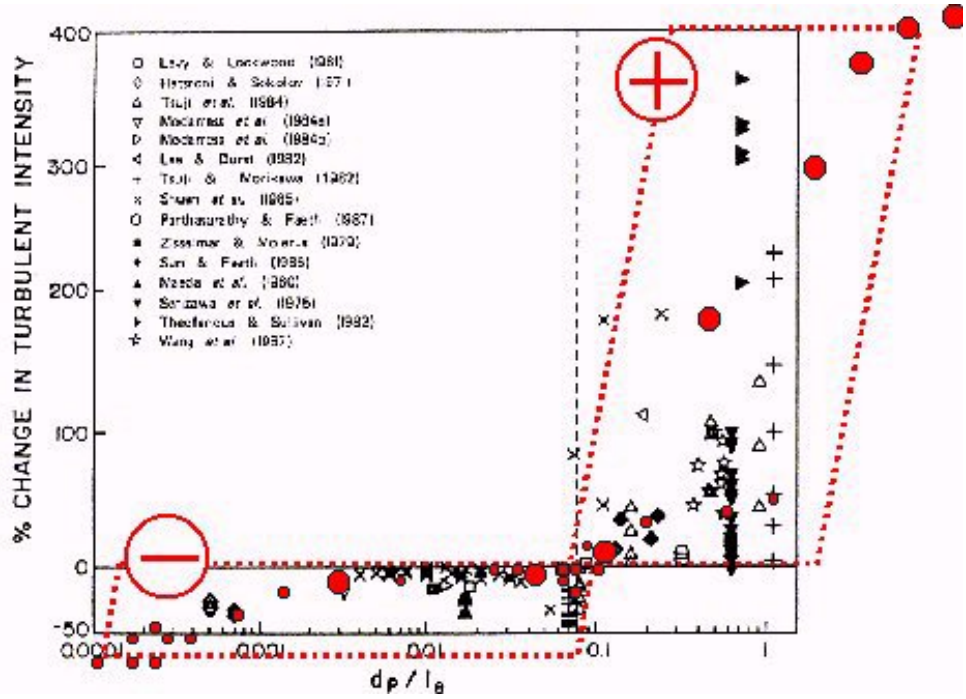

Figure 8.6: Turbulent intensity changes due to the droplets

8.2 Lateral wind

Another application of the PTV-Sizing technique to study turbulence changes is the use of a wind tunnel inside which a ramp of sprays is discharging perpendicularly to the mean flow. The initial turbulence of the gas is quite small and has been measured by LDV.

8.2.1 Experimental setup

Wind gallery

In order to carry out the experimental benchmark required to validate the two-phase flow code, a wind gallery is used to produce lateral wind when discharging water droplets. A sketch of the facility can be seen on Figure 8.7. Its width is 1.3m and its height is 1m. The free stream velocity is controlled with an anemometer placed far from the nozzles. Three different velocities have been chosen to perform the study, $0.25m.s^{-1}$, $0.50m.s^{-1}$ and $1m.s^{-1}$. As the scale of the nozzles is $1/5^{th}$ of real sprays, this scaling is also applied to the wind velocity. Therefore, the simulated wind corresponds to a real velocity of $5m.s^{-1}$. Above this limit, the dispersion of toxic cloud is mainly governed by pollutant dispersion in atmosphere, and the water curtains are not useful, as presented by St-Georges *et al.* (1992).

Water sprays

The water curtain is made by nozzles producing a flat fan spray. Their equivalent diameter is $d_0 = 0.53mm$ and their flow number is 8.1 $10^{-9}m^3.s^{-1}.Pa^{-1/2}$. The feeding pressure during the experiments is either 150kPa or 300 kPa. For the first pressure, the typical droplet diameter is about $220\mu m$, whereas for the higher pressure, it drops down to $150\mu m$. Those characteristics have been measured both by PDA (phase Doppler anemometer) and PTV-Sizing, as presented by Zimmer & Buchlin (1999). The spacing between the nozzles is 45mm or 90mm and they are placed at 50cm from the wall.

8.2.2 Mean velocity

To compute mean velocities with PTV results, one should not interpolate a mean velocity for all set of images, but more the mean velocity resulting from all the displacements found for a same test condition. The interpo-

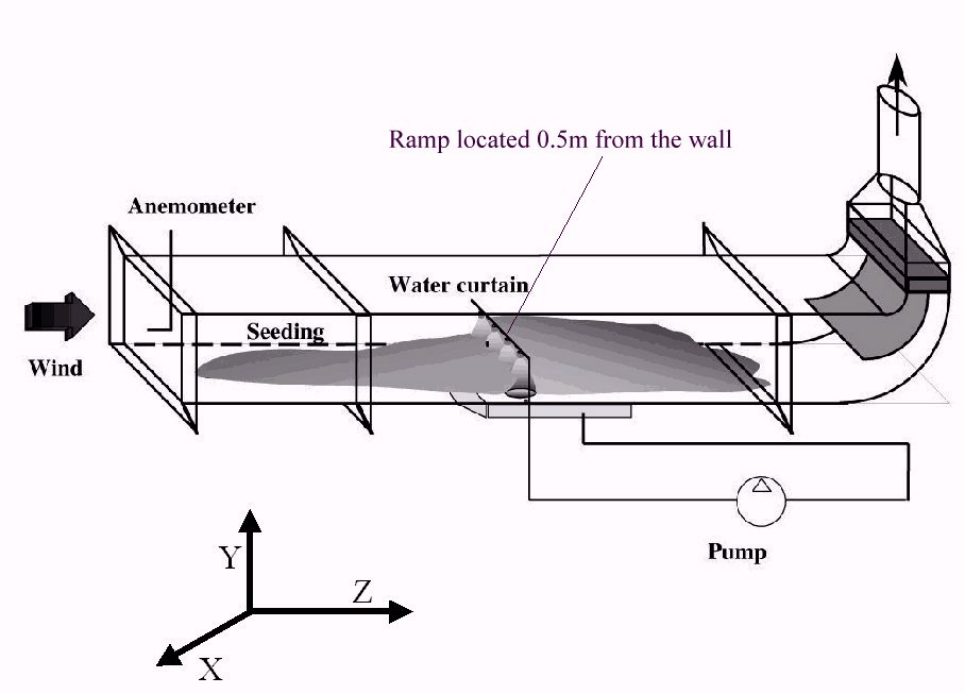

Figure 8.7: Schematic view of the experimental setup

lation using Adaptive Gaussian Window (AGW) on all the images can be formulated according to the following equation.

$$\langle V_i \rangle = \frac{\sum_p exp\left(-\frac{x_{pi}^2+y_{pi}^2}{h^2}\right) V_{pi}}{\sum_p exp\left(-\frac{x_{pi}^2+y_{pi}^2}{h^2}\right)} \tag{8.1}$$

The reason for this procedure is that if the average is performed image by image, this would give the same weight to all the images, regardless of the real position of the displacements found.

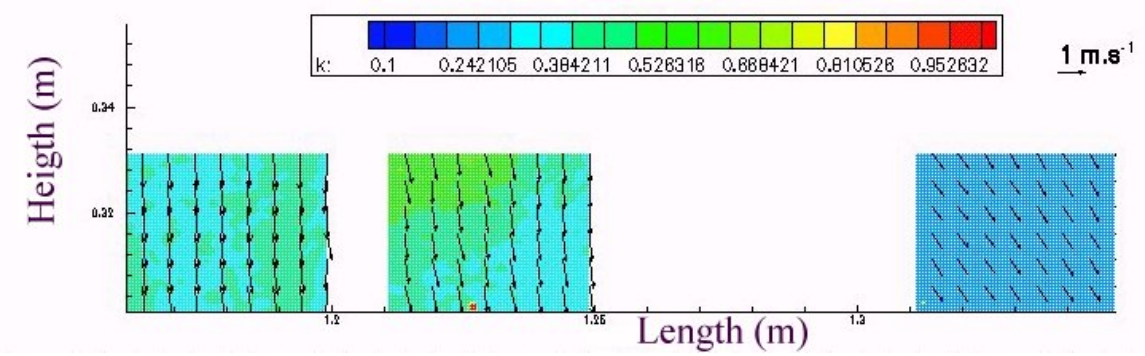

Figure 8.8: Mean and fluctuating components of the velocity

8.2.3 Comparisons with numerical predictions for the turbulent kinetic energy

A Navier-Stokes code coupled with a Lagrangian tracking for the water droplets is available to compute the mean and turbulent quantities of the flow. This code, validated by means of LDV upstream the water barrier (Zimmer (2001)) is used to compare the results obtained downstream the water curtain.

Streamwise position	$< V_3 > (m.s^{-1})$	$< V_2 > (m.s^{-1})$	k $(m^2.s^{-2})$	Type of results
1.18	0.34	-1.26	0.46	Numerical simulation
	0.11	-1.31	0.38	PTV-S
1.25	0.34	-1.04	0.42	Numerical simulation
	0.17	-1.02	0.43	PTV-S
1.33	0.47	-0.65	0.33	Numerical simulation
	0.36	-0.52	0.23	PTV-S

Table 8.1: Comparison between PTV-Sizing and the numerical computations

8.2.4 Size distribution

As PTVS gives also the size of the discrete phase, it is possible to compute the size distribution for different lateral velocity. This has been done for a position 25cm after the curtain and at 30cm from the lower wall. The results presented in figure 8.9 show an increase of the size of the droplets carried out by the mean flow induced by the water sprays and the air-stream velocity. This is also in concordance with the numerical results (Zimmer (2001)).

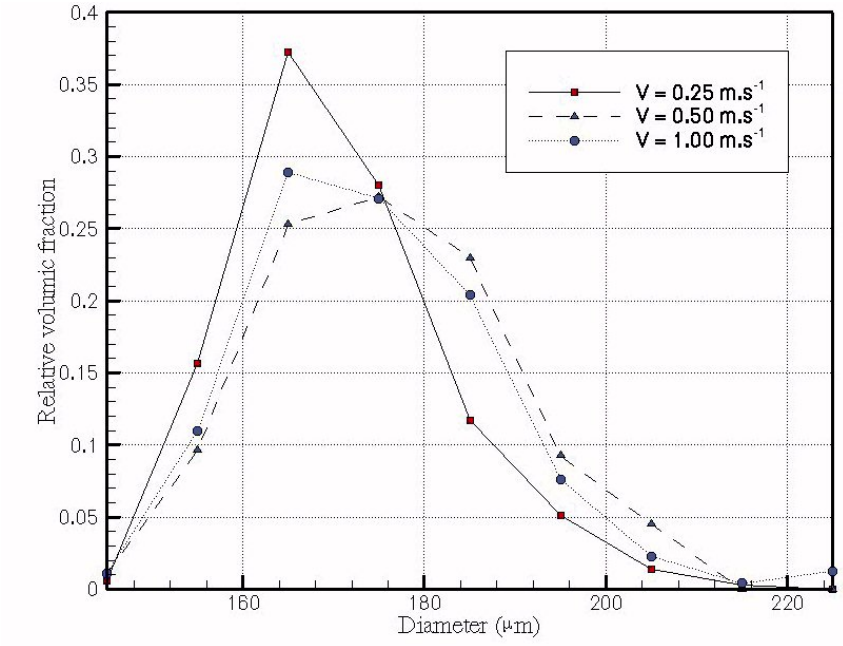

Figure 8.9: Probability density function of the droplets 25cm after the spray, obtained by PTV-Sizing

Chapter 9

Conclusions

This lecture proposed an introduction to tracking techniques. Three main steps are required to develop such a technique. the automatic detection of particles is the first step, and has to be carefully done to avoid noisy information. The second step is the digital sizing of the particles. Afterwards, to track individual particles, hybrid schemes using correlation techniques to limit the research area can be used. An important feature is to take into account the size information to enhance the reliability of the pairing process. Synthetic images have showed the good behavior of the tracking scheme. Applying tracking to real lungs bifurcations, the steady streaming displacement can be measured, and difference with integrated PIV fields can be seen. As far as two-phase flows are concerned, PTVS applied to real sprays shows good results for size distribution measurement, as well as for velocity. Furthermore, PTVS can be used as a discrimination process in case of the presence of the two phases on the images. Turbulence modification due to droplets can be measured by means of PTVS.

Bibliography

Agui, J. & Jiménez, J. 1987 On the performance of particle tracking. *Journal of Fluid Mechanics* **185**, 447–468.

Bachalo, W. & Houser, M. 1984 Phase/doppler spray analyzer for simultaneous measurement of drop size and velocity distributions. *Opt. eng.* **23**, 583–590.

Cenedese, A. 2000 Particle tracking velocimetry : measuring in the lagrangian reference frame. In *Particle Image Velocimetry and Associated techniques. Lecture Series 2000-01* (ed. R. M.L.). von Karman Institute for Fluid Dynamics.

Etoh, T., Okamoto, K. & Takehara, K. 1998 The particle mask correlation method. In *Eight International Symposium on Flow Visualization, Sorrento-Italy*.

Giannoulis, D. 1999 Spray droplet characterization by rainbow interferometry using a laser sheet. *DC-Report 99-09, von Karman Institute for Fluid Dynamics* .

Gore, R. & Crowe, C. 1989 Effect of particle size on modulating turbulence intensity. *Int. J. Multiphase Flow* **15** (2), 279–285.

Herpfer, D. & Jeng, S. 1995 Streaked particle image velocimetry and sizing in a spray. *Atomization and Sprays* **5**, 403–416.

Herpfer, D., Jeng, S. & Jeng, S. 1995 Comparison of spivs to pdpa measurements in a nonreacting spray. *SPIE* **2546**, 65–74.

Ikeda, Y., Yamada, N., Kawahara, N., Shimo, D. & Nakajima, T. 1998 Piv application fro spray characteristic measurement. In *Ninth International Symposium on applications of laser techniques to fluid mechanics*. Lisbon, Portugal.

Kim, J., Cho, J. & Lee, S. 1999 Improvement of pattern recognition algorithm for drop size measurement. *Atomizations and Sprays* **9**, 313–329.

Kobayashi, T., Kawaguchi, T. & Maeda, M. 2000 Measurement of spray flow by an improved interferometric laser imaging droplet sizing (ilids) system. In *Tenth International Symposium on applications of laser techniques to fluid mechanics,Lisbon,Portugal*.

Marxen, M., Sullivan, P., Loewen, M. & Jähne, B. 2000 Comparison of gaussian particle center estimators and the acievable measurement density for particle tracking velocimetry. *Experiments in Fluids* **29** (2), 145–153.

Ohmi, K. & Li, H. 1999 Particle tracking velocimetry applied to a wind tunnel flow past a single row of circular cylinders. In *3rd International Workshop on Particle Image Velocimetry*. Santa Barbara - California.

Ohmi, K. & Li, H. 2000 A new particle detection method for particle tracking velocimetry. In *9th International symposium on flow visualisation*. p. 6.

Ohmi, K. & Yoshida, N. 2000 A new type of ga-based particle tracking velocimetry. In *9th International symposium on flow visualisation*. p. 7.

Okamoto, K., Nishio, S., Saga, T. & Kobayashi, T. 1997 Standard images for particle imaging velocimetry. In *PIV-Fukui'97*. pp. 229–236.

Prétrel, H. 1997 étude du comportement thermohydraulique de pulvérisations liquides sous l'effet d'un rayonnement infrarouge. PhD thesis, École Doctorale des Sciences de l'Ingénieur de Lyon.

Ramuzat, A., Richard, H. & Riethmuller, M. 1999 Piv investigation of unsteady flows within lung bifurcations. In *8th international conference on Laser Anemometry Advanced and Applications*. Roma - Italy.

Ramuzat, A. & Riethmuller, M. 2000 Etude des écoulements pulmonaires dans un modèle tridimensionnel de bifurcations multiples.

Scarano, F. & Riethmuller, M. 1999 Iterative multigrid approach in piv image processing with discrete window offset. *Experiments in Fluids* **26**, 513–523.

St-Georges, M., Buchlin, J.-M., Riehtmuller, M., Lopez, J., Lieto, J. & Griolet, F. 1992 Fundamental multidisciplinary study of liquid sprays for absoprtion of pollutant or toxic clouds. *TransIChemE* **70**, 205–213.

Suda, J. 2000 Experimental investigation on turbulence modification by particles in shear layer flow using l-6 twin-jet wind tunnel. *PR2000-20 von Karman Institute for Fluid Dynamics* .

Suda, J., Zimmer, L. & Buchlin, J.-M. 2001 Experimental investigation on turbulence modification by droplets in shear layer flow. *ICMF-2001* .

VanBeeck, J. 1996 Rainbow phenomena: development of a laser-based, non-intrusive technique for measuring droplet size, temperature and velocity. PhD thesis, Eindhoven University of Technology.

VanBeeck, J. & Riethmuller, M. 1996 Rainbow phenomena applied to the measurement of droplet size and velocity and to the detection of non-sphericity. *Applied optics* **35** (13), 2259–2266.

Westerweel, J. 1994 Efficient detection of spurious vectors in particle image velocimetry data. *Experiments in Fluids* **16**, 236–247.

Zimmer, L. 2000 Particle tracking velocimetry and sizing technique in two-phase flows. In *Particle Image Velocimetry and Associated techniques. Lecture Series 2000-01* (ed. R. M.L.). von Karman Institute for Fluid Dynamics.

Zimmer, L. 2001 étude expérimentale et numérique de la turbulence en écoulement diphasique. applications aux rideau d'eau en présence de vent latéral. PhD thesis, Université Henri Poincaré de Nancy - Université Libre de Bruxelles.

Zimmer, L. & Buchlin, J.-M. 1999 Particle tracking velocimetry and sizing technique for studying mixing of sprays. In *15th Annual Conference on Liquid Atomization and Spray Systems*. Toulouse.

Zimmer, L., VanBeeck, J., Santonastasi, M. & Riethmuller, M. 2000 Simultaneous measurement of mean droplet size and temperature within a flat fan spray by global rainbow thermometry. In *16th Annual Conference on Liquid Atomization and Spray Systems*.